An energy management system for ships with electric propulsion and a modular hybrid power supply

W. van Schie

TU Delft

Thesis for the degree of MSc in Marine Technology in the specialization of *Ship Design / Marine Engineering*

An energy management system for ships with electric propulsion and a modular hybrid power supply

By

W. van Schie

Performed at

Marin

Thesis number: MT.24/25.002.M

27 September 2024

Company supervisors
Responsible supervisor: Dr. Ir. U. Shipurkar

Thesis exam committee
Chair/Responsible Professor: Dr. Ir. H. Polinder
Staff Member: Dr. A. Coraddu
Staff Member: T. Kopka
Company Member: Dr. Ir. U. Shipurkar

Author Details
Student number: 4445104

Cover photo [1]

Abstract

To reduce the greenhouse gas emissions of ships, hybrid power systems are becoming more common. Hybrid systems combine power generation with energy storage. The energy storage enables the power generating components to run at more efficient operating points. A well known combination is that of a diesel genset and a battery. The ideal combination of the type, size, and amount of power system components depends highly on the operating profile of the vessel. However, this operating profile can vary greatly between voyages, or during the lifetime of a vessel, thus changing the 'ideal' power plant. A modular power system (MPS) can provide the solution: a reconfigurable power plant, where components can be added, removed, or replaced.

To control the power-split between the different components an energy management system (EMS) is required. Most EMSs are designed and optimized for a single power plant configuration. This means they are not capable of dealing with an MPS. For this thesis an EMS was developed which is capable of dealing with an MPS: an MPS EMS. The developed EMS was made for ships with electric propulsion. An additional requirement was for the EMS to be real-time capable, so it can be used outside of a simulated environment, i.e. in a real ship. The objective of the EMS would be to minimize fuel consumption.

It was investigated which EMS control strategy would be suited for an MPS EMS. The equivalent consumption minimization strategy (ECMS) combined with the dual decomposition method was found to be suited for this purpose.

The developed EMS can automatically adapt all parameters responsible for stable control of the system. It does this based on the properties of the installed components. Most important of these properties are: minimum and maximum power output, maximum ramp-rate, and the efficiency curve.

The EMS was tested with four different combinations of installed components, and two different operating profiles. Additionally, the effect of a component failure during a voyage was tested. A rule based (RB) EMS and a mixed integer linear programming (MILP) global optimization were used as benchmarks for the fuel consumption. The results show that the developed EMS is capable of controlling various power plant configurations in different conditions, while keeping all components within their allowed operating ranges. For one of the tested operating profiles the fuel consumption using ECMS was 1.9-2.3% higher than when using the global optimization, which is comparable to the results found in literature. However, for the other tested operating profile the developed EMS was outperformed by even the RB EMS, by 1.1-2.1%. This was caused by inaccuracies of the approximation used for the efficiency curve of the gensets. In the simulations where one of the gensets fails during the voyage the EMS was able to automatically adapt to optimize fuel consumption using only the remaining components. Fuel consumption did increase slightly compared to no failures, as expected.

Keywords: Energy management system, modular power system, ECMS, dual decomposition, shipboard power system, electric propulsion

Nomenclature

Abbreviations:

BSFC	break specific fuel consumption
CD/CS	charge depleting/charge sustaining
ECMS	equivalent consumption minimization strategy
EMS	energy management system
ESS	energy storage (system)
FMU	functional mock-up interface
GHG	greenhouse gas
ICE	internal combustion engine
MILP	mixed integer linear programming
MPS	modular power system
OP	operating profile
RB	rule based
SoC	state of charge

Symbols:

a	power of the cost-factor penalty function
m_{fuel}	fuel mass / cumulative fuel consumption
Q	lower heating value (of diesel)
u	power input (of a module)
v	total load power/required power
y	power output (of a module)
α	step size for the steepest ascend method
$\in$	convergence criterium
η	efficiency
λ	equivalent cost factor
μ	Lagrange dual variable/Lagrange multiplier
τ	size of the EMS time-step

Subscripts:

m	the module/component

Superscripts:

s	iteration number

List of figures

List of tables

Table of content

1 Introduction

1.1 Background

The shipping sector is responsible for 3% of global CO2 emissions [2], [3]. The shipping industry is expected to keep growing, thus only further increasing its environmental impact. To reduce emissions, a reduction in fossil fuel consumption is necessary. Regulation imposed by the International Maritime Organization (IMO) Marpol are getting increasingly stringent [4], [5]. Given these regulations as well as the increasing price of energy, it becomes necessary that technologies are developed to reduce the fuel consumption and emissions of ships.

One promising technology is the use of hybrid power systems. This is primarily beneficial for ships with operating profiles which have periods of high power demand, as well as periods of low power demand [6], [7]. Hybrid ships can run their power generating components, such as internal combustion engines (ICE) and fuel cells (FC), at a more fuel efficient operating point. An (electric) energy storage system (ESS) stores or provides additional power [8]. Using hybrid power systems can also provide other benefits, such as improved reliability, quieter operation, and reduced maintenance costs [9]. A downside of hybrid power systems is the increased complexity and costs of the physical system, as well as the control system.

The power plant of a vessel is designed with the expected operating profile in mind [10]. However, the operating profile can vary greatly between missions, due to environmental influences (such as wind, waves, and currents) and operational conditions (e.g. the frequency of the required actions of the vessel, such as loading or unloading cargo, sail across open sea or towing another vessel) [11]. This means the 'ideal' power plant will not be the same for each mission. Here, a modular power system (MPS) would provide a solution: a reconfigurable power plant, where components can be added, removed, or replaced.

To achieve the benefits possible with (modular) hybrid systems, the different components need to work together. For this an energy management system (EMS) is required. The EMS controls how much power each component delivers. The EMS ensures that supply matches demand, and that each component stays within its safe operating range. Other possible goals are extending component lifetime, failsafe operation, reducing greenhouse gas (GHG) emissions, and minimizing fuel consumption [12], [13]. Which goal(s) the EMS aims to achieve influences its decision making.

Most EMSs are developed in parallel with a vessel, and its power plant and operating profile. As such, these EMSs would need to be re-designed if the vessel is ever retrofitted with a different power plant, and/or gets a new purpose with a different operating profile. This is also the challenge with an MPS. The EMS can not be developed for one single power plant configuration, and one operating profile. An EMS for an MPS needs to be able to perform its task, regardless of the power plant configuration and operating profile. The use of such an EMS could also improve reliability: in the case where one of the installed components fails, the EMS will automatically adjust to optimize the power split for the remaining components.

This master thesis project focusses on developing an EMS for an MPS. This MPS EMS is applied and tested in a simulated environment. The component models and the operating profiles, that were provided are part of the MENENS project [14]. These models represent a luxury yacht with a

length of 84 meters. Which power components are connected will be varied, to verify the performance of the EMS for an MPS.

1.2 Research goal and research questions

The goal of this research is to develop an EMS, which is capable of dealing with a modular hybrid power system in real-time. The developed EMS needs to be able to minimize fuel consumption, regardless of the amount and type of power generating/storing components are used, and for any operating profile (given that the installed components are capable of matching demand). For this project, an MPS on a ship with electric propulsion is considered. The choice for electric propulsion was made during a literature study, and will be explained in chapter 2.

In order to reach the described goal, the following research question was formed:

> *How can a shipboard modular power system be controlled, such that fuel consumption is minimized?*

Multiple sub research questions were formed in order to help answer the main research question:

1. What control strategy is suited for such an EMS?
2. How can a variable number/type of connected components be represented in the controller?
3. How can the performance of the developed EMS be assessed?

1.3 Contribution

This research provides a novel energy management approach for ships with electric propulsion and a hybrid power plant. An EMS which can perform well, in terms of minimizing fuel consumption, for any combination of power components, and for any operating profile. The developed EMS is mainly meant for MPSs, but can also be useful for other applications. It can be used as a benchmark during development of a bespoke EMS, or as a tool to find a good power plant configuration during the development of a vessel. Another use case is in retrofitted vessels, bypassing the need to develop a bespoke EMS and the associated costs.

1.4 Report outline

Chapter 2 shows the findings of the a previous literature study performed on this topic [15]. This includes the properties of the different propulsion topologies, and why electric propulsion was chosen for this research. As well as which control strategies exist and which would be suited for a modular system.

Chapter 3 describes the system that is used for this thesis. Both the overall system, and the models used for the different components.

Chapter 4 shows the process inside the developed EMS, and how modularity of the power system was accommodated for. A description of the benchmark methods (a global optimization, and a rule based (RB) EMS) is also given.

Chapter 5 shows the simulation results, and discusses the observations made on them. Furthermore, the results are compared to the benchmarks.

Finally, in chapter 6 the conclusions of this research are drawn.

2 Literature study

As part of this thesis a literature study was done [15], to get an overview of research that has been done in the field of EMS, and to make an informed decision regarding which propulsion topology this thesis should focus on. In this chapter the findings of the literature study are presented. Section 2.1 shows the different propulsion topologies, and why it was decided to develop an EMS for electric propulsion. Section 2.2 explains the different EMS control strategies.

2.1 Power systems

During the literature research it was investigated which propulsion topology would benefit most from an MPS. Figure 1 shows the three main propulsion topologies: mechanical, hybrid, and electrical.

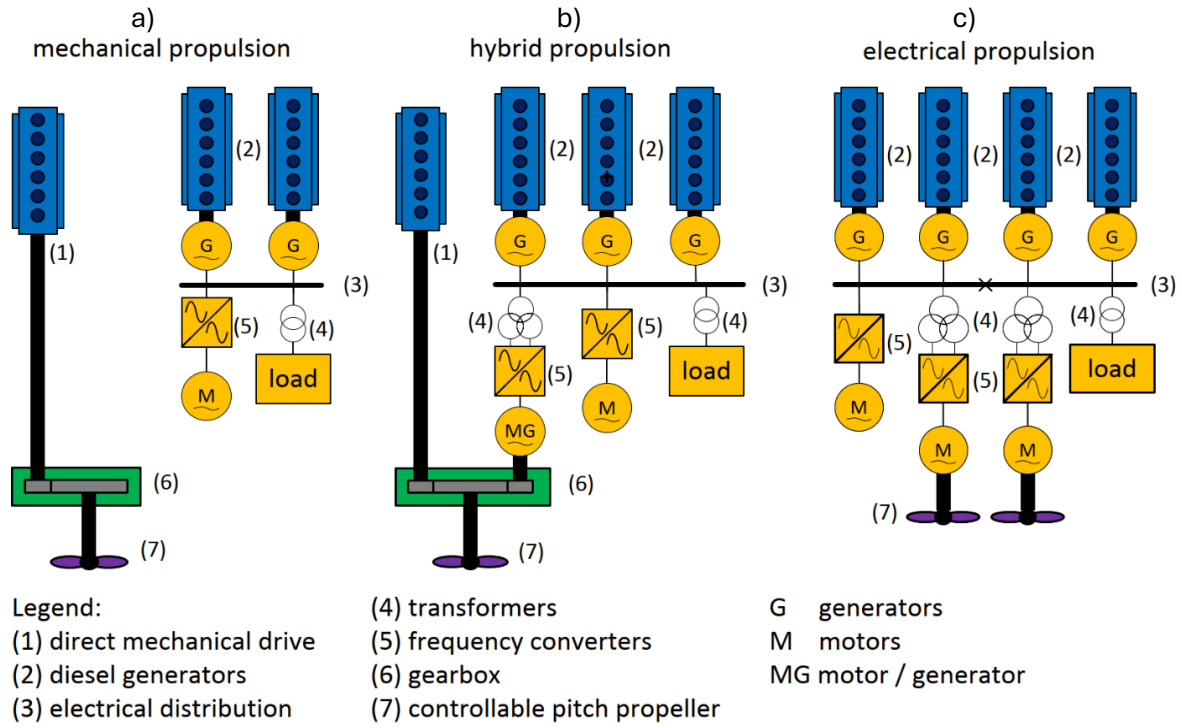

Figure 1 Schematic representation of propulsion architecture qualification. From [4]

2.1.1 Mechanical propulsion

Mechanical propulsion (Figure 1a) has minimal energy conversion stages, which means minimal energy losses. However, high fuel efficiency can only be achieved if the engine and propeller can be run close to the designed operation point. Diesel engines operate most efficiently at high loads [16]. Therefore, mechanical propulsion is very suitable for ships with a mainly constant propulsion power profile at high load. One common ship type that has this characteristic is ocean-going cargo ships.

2.1.2 Electrical propulsion

With electrical propulsion (Figure 1c) the propellers are only driven by electric motors and are not mechanically connected to ICEs. Because there are multiple energy conversion stages, electrical propulsion has a lower peak fuel efficiency than mechanical propulsion [9]. The amount of active generators can be controlled. This makes it possible to avoid running generators at inefficient

operating points [17]. This topology is well suited for ships which have high hotel loads and a varying load profile, such as cruise ships [18].

Contrary to mechanical propulsion, the propulsion power does not necessarily need to be provided by ICEs. Batteries, FCs, or a combination of different power supplies is also possible, as can be seen in Figure 2. This makes it possible to create a ship with zero GHG emissions.

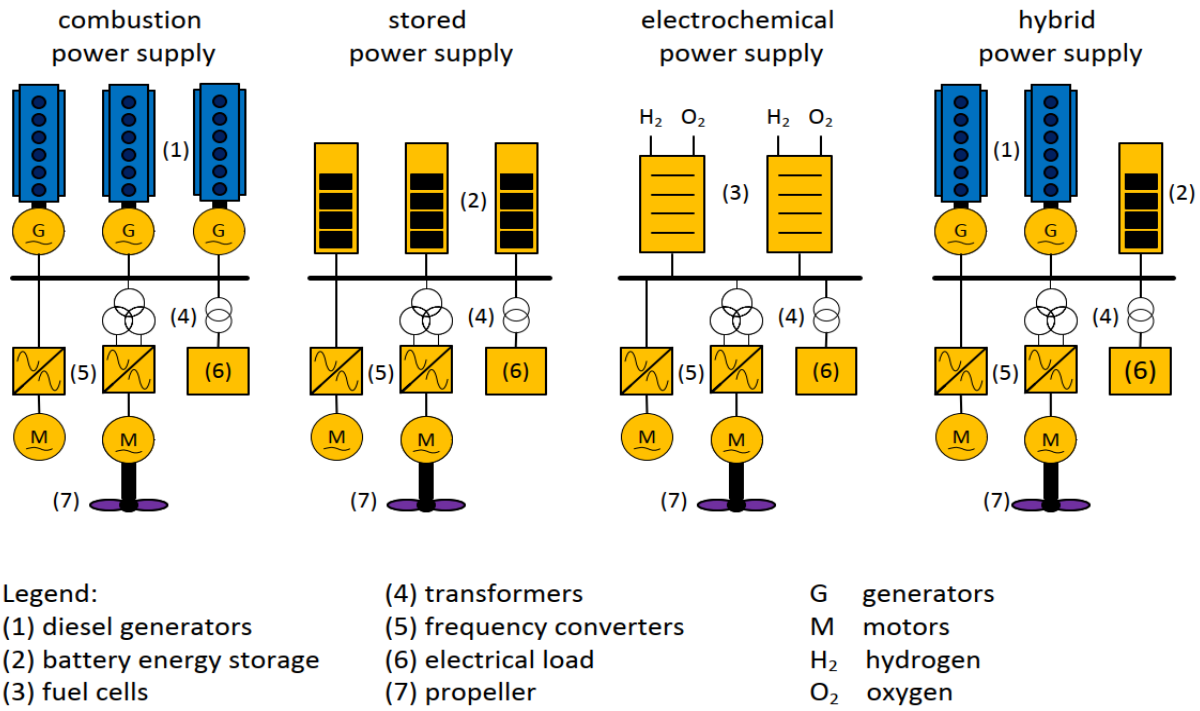

Figure 2 Schematic representation of power generation architecture qualification. From [4]

2.1.3 Hybrid propulsion

Hybrid propulsion (Figure 1b) combines mechanical and electrical propulsion. The propeller is mechanically connected to both an ICE and an electric motor. This topology is beneficial when a ship often operates below its design speed [6]. One downside of hybrid propulsion is the added complexity from connecting the different components. It also requires a robust control system to regulate the torque-split between the electric motor and the ICE [9], [19].

2.1.4 Modularity

There are some papers that discuss MPS. However, most studies do not fully agree on what 'modular' means. [20] defines 'modular' as being the presence of multiple of the same power source, instead of one larger power source. I.e. multiple fuel cell stacks, or multiple gensets. Notably, only examples with electric propulsion are shown. Although [20] does not mention the challenges of controlling such systems, it does discuss the practical benefits. These benefits include: improved efficiency, redundancy, flexible mass distribution, and reduced production cost. In [11] 'modular' means reconfigurable, similar to the definition in this report. This is then applied to the ESS of a tugboat with hybrid propulsion, as shown in Figure 3. The amount and size of the installed batteries can be changed each voyage.

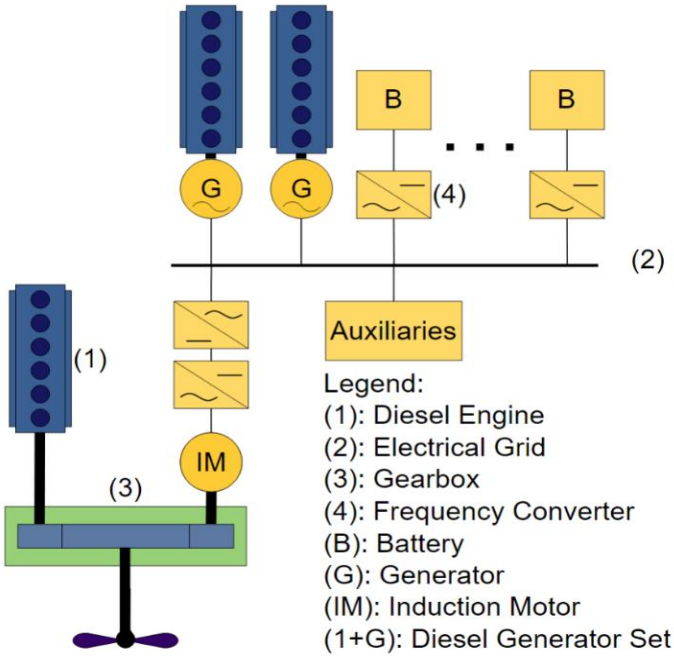

Figure 3 Power plant for modular control architecture. From [11]

An engine that is mechanically connected to the propeller is specifically chosen/designed to match the characteristics of the propeller, and can not easily be replaced. Therefore, it is not practical to make this component part of the MPS. For the electrical power system each individual power component can be switched off and on. New components can also be connected. This means it is possible to implement an MPS to the electrical power system. Therefore, implementing an MPS will not be beneficial if the majority of required power is mechanical. Additionally, an MPS will mainly benefit vessels with a varying operating profile [11]. Based on this, mechanical propulsion is ruled out for an MPS, while ships with electric propulsion would benefit most [9], [16].

2.2 EMS control strategies

Many different EMS control strategies exist. These control strategies can be categorized into three groups: Rule based, optimization based, and learning based [21], [22]. Figure 4 shows control strategies found in literature. All strategies shown in Figure 4 are discussed in [15]. The strategies that are important for this project are discussed below.

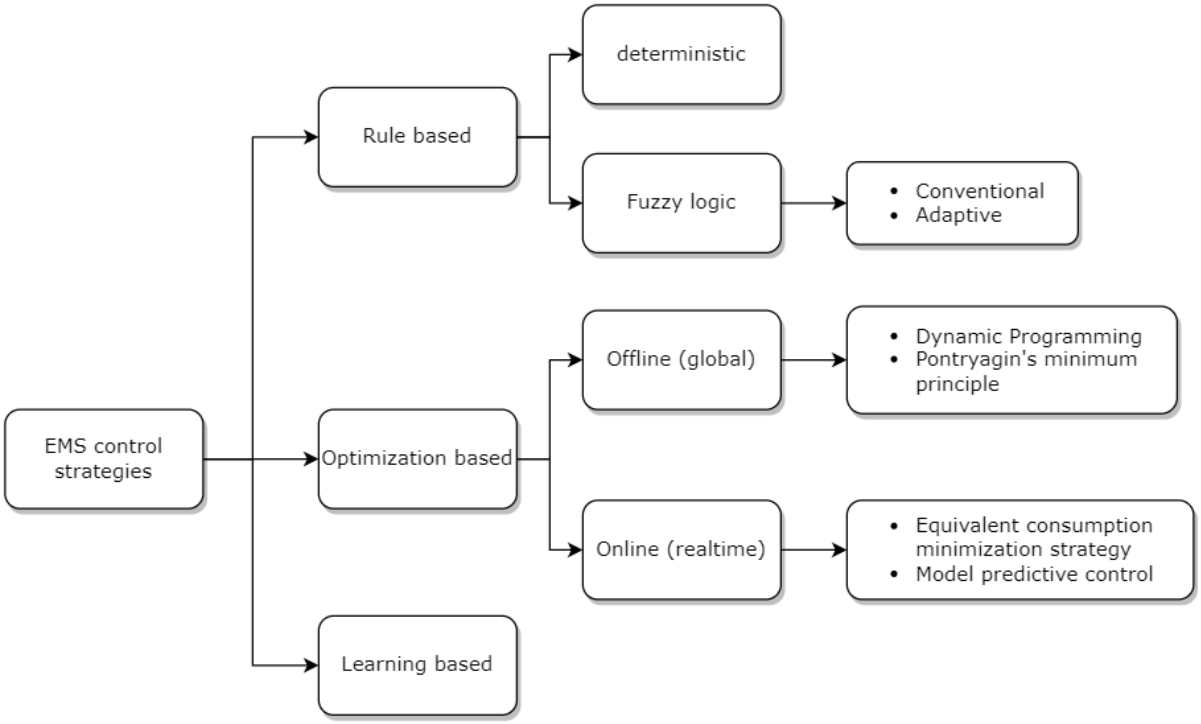

Figure 4 EMS control strategies divided by category

2.2.1 Rule based

A great benefit of rule based (RB) strategies is that they are easily implementable in real-time applications. They do not have to run any kind of optimization, but simply rely on a set of rules to decide the output values of the EMS. This, combined with their robustness, makes RB EMSs popular in the industry. Intuition and knowledge of the optimal global solution are used to determine which rules to apply [22], [23]. This is shown in [24], where dynamic programming is used to find the optimal solution from which implementable rules are then derived. RB EMS are each developed for a specific vehicle/vessel. If the power system configuration is changed, rules will need to be tuned, added, or removed.

2.2.2 Online optimization based

Online methods solve an instantaneous optimization problem at each time instant [23]. The complete operating profile/driving cycle is not known to the system. Only information about the current and previous system states is used. It is possible for online methods to run simulations at (faster than) real-time speed. This makes them suitable for real-time implementations.

One such control strategy is the equivalent consumption minimization strategy (ECMS). With ECMS a cost factor is assigned to the energy stored in the battery, such that its cost is roughly equivalent to that of the fuel which was consumed to generate it [22], [23]. The equivalent fuel consumption is then minimized at each time instant. In [25] a dual decomposition method is applied so the optimization can be done for each sub-system individually.

2.2.3 Offline optimization based

Offline methods only work in a simulated environment. They require the full operating profile/driving cycle to be known a priori, while online methods do not need any knowledge of the future. Because of this, offline methods can provide a better solution than online methods.

Although offline methods cannot be used for real-time implementations, they can be a very useful tool. They can be used as benchmark solutions when designing and optimizing other control strategies [13], [21], [22]. Another way to use offline methods, is to have them create/tune rules or look up tables for real-time applications [26].

Some common offline methods are dynamic programming [19], [23], [27], [28], Pontryagin's minimum principle [29], [30], [31], and mixed integer linear programming (MILP) [32], [33], [34].

2.3 Conclusions

It was concluded that the electric propulsion topology could benefit most from a modular power system. therefore, this thesis focusses on developing on an MPS EMS for ships with electric propulsion. For the control strategy, it was found that the method of combining ECMS with dual decomposition, as used in [25], is very well suited for use in an MPS EMS.

3 System description

This chapter gives a description of the system that is controlled by the EMS. As stated, the system for this project uses the electric propulsion topology, as shown in Figure 5. The operating profile and installed power are for a luxury yacht with a length of 84 meters, and a gross tonnage of 2554. Yachts generally do not have a fixed operating profile, both in terms of length, and of how much time is spent performing tasks. Such a variable operating profile makes yachts ideal candidates for MPSs.

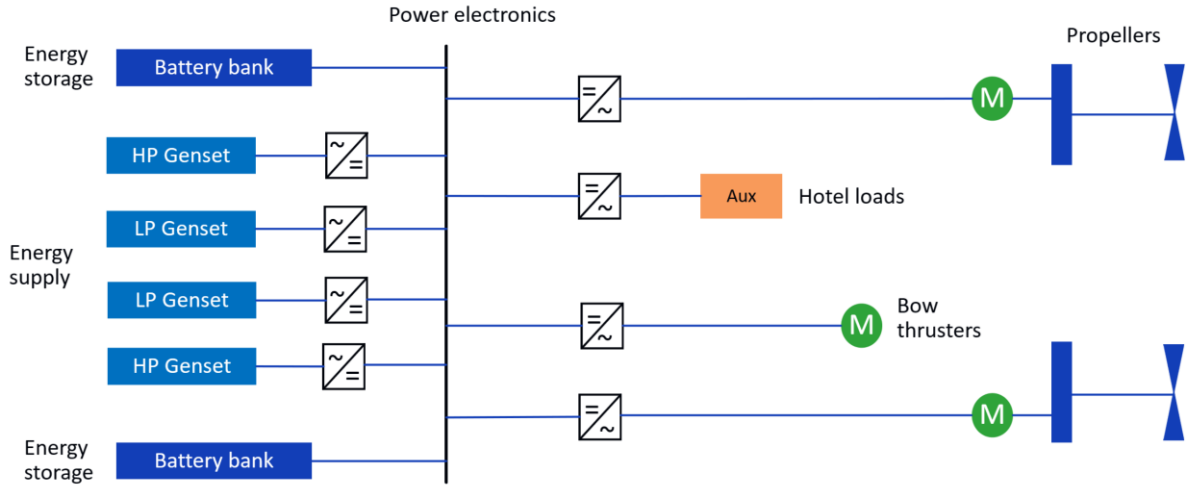

Figure 5 topology of a ship with electric propulsion [14]

3.1 Operating profile

Using electric propulsion means the propeller speed does not directly influence the torque load and rotational speed of any ICE. The only influence of the propeller on the energy system (through the electric motor) is its electric power requirement. This makes it possible to model the operating profile (ship speed, hotel loads, auxiliary loads) simply as total required electrical power.

Figure 6 and 7 show typical operating profiles for a luxury yacht, made in collaboration with the MENENS project [14]. Operating profile 1 is for a 36 hour voyage. It consists of fast cruising, fast cruising in sea state 3, economic cruising, economic cruising in sea state 3/6, sailing at top speed, regular cruising, and being berthed/anchored. The highest power demand is 4116 kW.

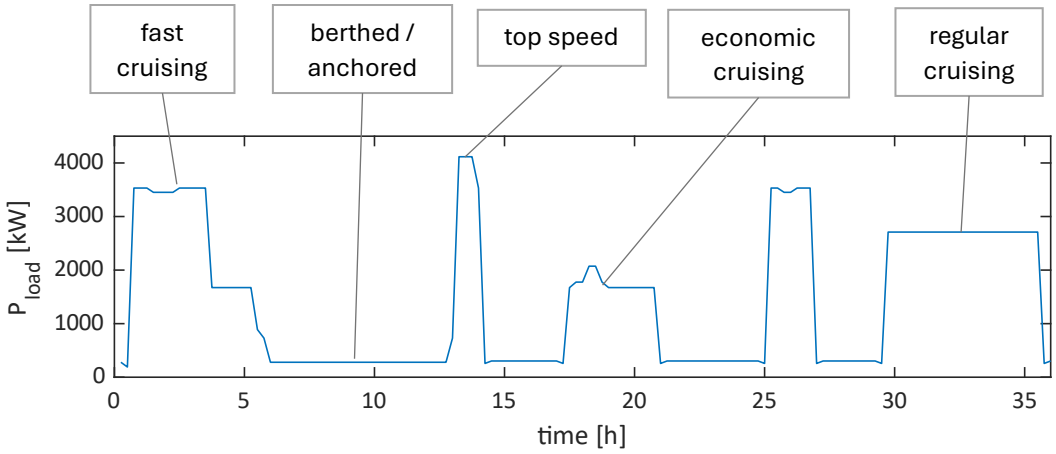

Figure 6 Operating profile 1, a 36 hour voyage of a luxury yacht

Operating profile 2 is for a two week voyage. It consists mostly of fast cruising, economic cruising, and economic cruising in sea state 3/6. The highest power demand is 3475 kW.

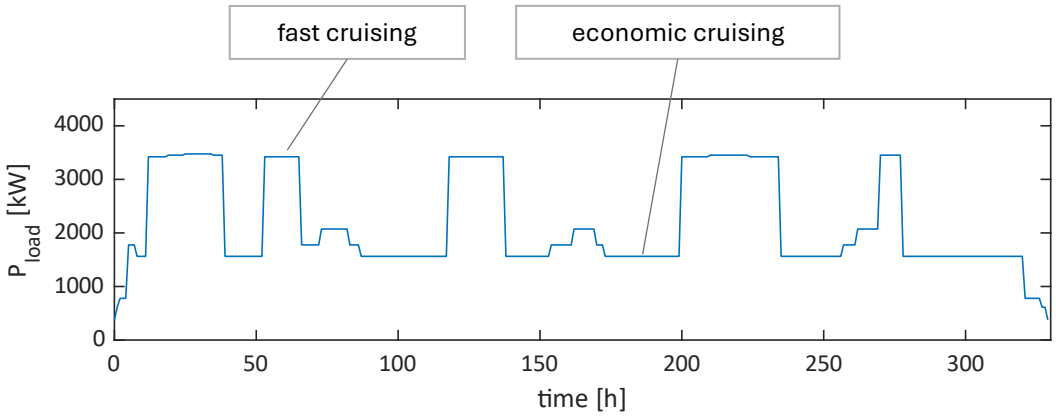

Figure 7 Operating profile 2, a two week voyage of a luxury yacht

3.2 Component models

The Simulink models of the gensets and battery have been provided by TNO in the form of a functional mock-up interface (FMU). These are black-box models. The models were validated by TNO using real world measurements, and are assumed to be accurate enough for the purposes of this project. The genset models are based on the 895 kW CAT C32 and 1417 kW CAT C32B. The different gensets will be referred to as the LP (low power) and HP (high power) gensets respectively. The battery model is based on NMC (Lithium Nickel Manganese Cobalt Oxide) technology. Table 1 gives a short list of the used component models and their respective maximum power output. Table 2 and 3 show which parameters and inputs are required to use the FMUs, as well as the outputs.

Table 1 list of the used component models

Component	Based on	Max. power output
LP (low power) genset	CAT C32	825 kW
HP (high power) genset	CAT C32B	1290 kW
Battery	NMC battery	±1500 kW

3.2.1 Gensets

The main electric grid of the system uses DC technology. Therefore, variable speed gensets are used. Figure 8 shows the engine efficiency maps of both genset types. The cyan curve in the engine maps shows the most efficient operating point for the power output. This line is not continuous, and would also require the engine to operate at maximum torque when at high power. The discontinuities could cause large swings in engine speed for small changes in required power output. Operating at maximum torque would cause clipping of the provided engine controller. The red line was created to handle these issues, at the cost of a slight bit of efficiency. The swings in engine speed were spread over a larger range of power output. Torque was limited to 98% of the maximum. From the red curve, Figure 9 was created, which shows the power output and efficiency versus the power input (i.e. fuel flow). From Figure 9 it is clear that the LP genset is more efficient than the HP genset for most of its output range.

Table 2 parameters, input, and output of the genset FMU's

Parameters	**Input**	**Output**
Inertia of the engine [kg m^2]	ICE on / off[-]	Torque [Nm]
Inertia of the electric motor [kg m^2]	Required torque fraction [-]	Electric power output [W]
Rated efficiency of the generator [%]	Requested voltage output [V]	DC current output [A]
Proportional action for the speed control [-]	Desired genset speed [rad/s]	BSFC [g/kWh]
Integral action for the speed control [-]		Maximum electric power at current operating speed [W]
		NOx emission [g/kWh]

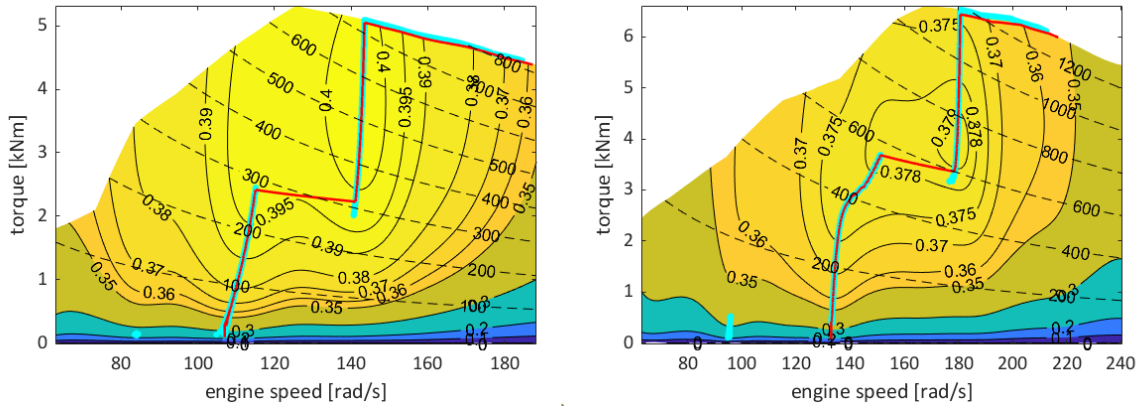

Figure 8 engine efficiency maps of the LP genset (left) and HP genset (right). The dashed lines are constant power [kW]. The cyan line shows the most efficient operating point for each power level. The red line shows a version of the cyan line where discontinuities and maximum torque are avoided.

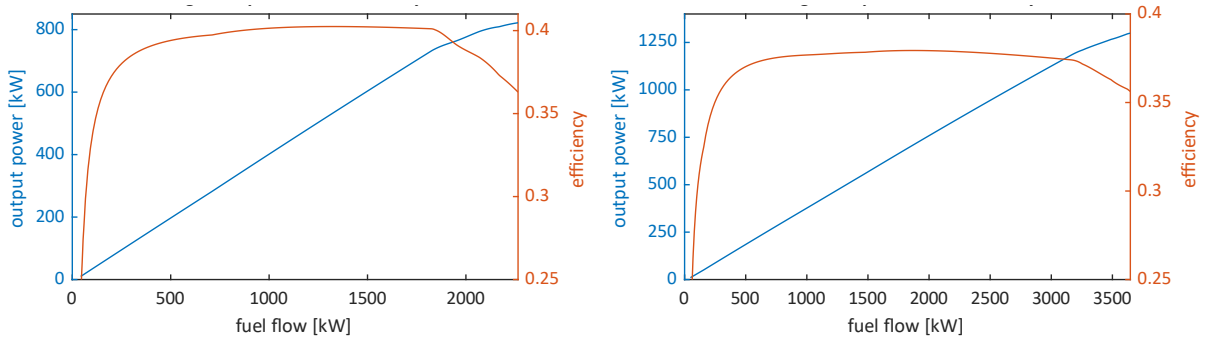

Figure 9 optimal power and efficiency curve for the LP genset (left) and HP genset (right)

3.2.2 Battery

The capacity and nominal voltage of the battery model are parameters which can be set by the user. The default values are a capacity of 5000 Ah and a nominal voltage of 805 V, which was sized for the application by [14]. Additionally, the maximum charge/discharge rate was set to 1500 kW. Through draining the battery at a very low discharge rate (in simulation), the energy capacity was found to be 4025 kWh for the set parameters. From the provided data Figure 10 was created, showing the efficiency as a function of SoC and power in-/output. Positive power is discharging, negative power is charging. Below an SoC of 35% the decrease in efficiency as a function of SoC seems to be linear, which is not as expected for an NMC battery [35]. However, this does not influence modularity of the system. Nevertheless, the lower bound SoC of the battery FMU was set to 35% during all its use.

Table 3 parameters, input, and output of the battery FMU

Parameters	Input	Output
Nominal capacity [Ah]	Current [A]	Pack voltage [V]
Nominal voltage [V]		Pack SoC [%]
Initial SoC [%]		SoC limit flag [-]
Upper bound SoC [%]		
Lower bound SoC [%]		

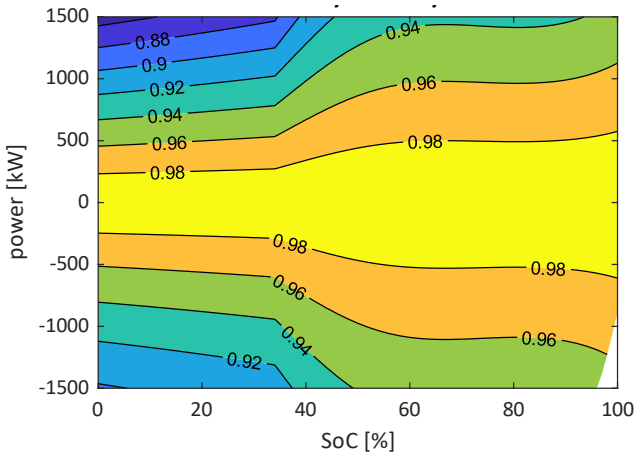

Figure 10 battery efficiency map. Positive power means discharging

3.3 Configurations

The power system configuration of the MENENS project consists of two LP gensets, two HP gensets, and two battery packs. This configuration will be used as the default configuration for this project.

To be able to scale genset size, the efficiency is normalized to be a function of the fraction of maximum power output. This scaling is used to be able to use various genset combinations, while keeping installed power constant. To be able to scale size of the batteries, the efficiency is normalized to be a function of the discharge rate. The result of making the models scalable is shown in Figure 11.

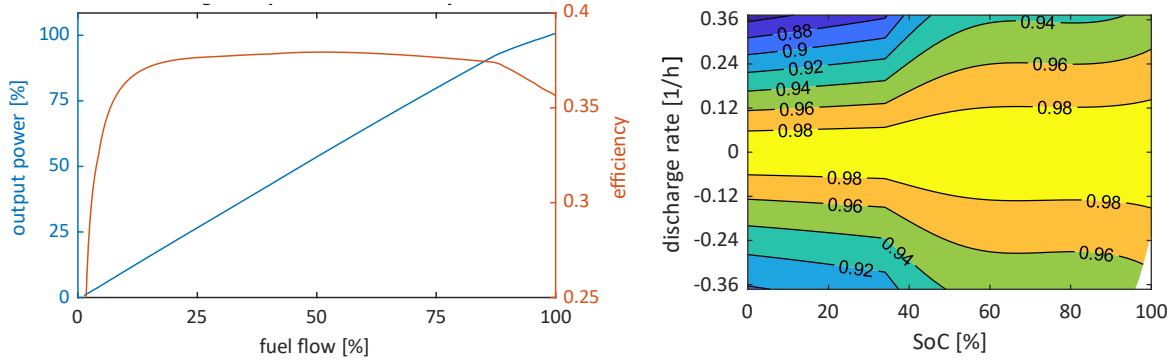

Figure 11 power and efficiency of the HP genset (left) and the battery (right) as a function of power fraction and discharge rate, respectively

Table 4 shows the different configurations that were used for testing the MPS EMS. For all tested configurations (with the exception of configuration 2), the installed genset power was kept the same at 4230 kW. This is higher than the maximum required power in either of the operating profiles, which ensures the system can always provide enough power, even when the batteries have been drained.

Configuration 1 is the default configuration. Configuration 2 corresponds to original configuration of the vessel used by MENENS. This will also show how the EMS performs when all connected gensets are identical. Configuration 3 will show how well the EMS can utilize larger batteries. Maximum battery power was kept equal. Configuration 4 was chosen to show the EMS can handle a different amount of connected gensets.

Table 4 all hardware configurations used to test the proposed EMS

Config	LP gensets	HP gensets	batteries
1	2x 825 kW	2x 1290 kW	2x 5000 Ah, 1500 kW
2	-	4x 1290 kW	2x 5000 Ah, 1500 kW
3	2x 825 kW	2x 1290 kW	2x 10000 Ah, 1500 kW
4	1x 1650 kW	1x 2580 kW	2x 5000 Ah, 1500 kW

4 EMS description

With the conclusions of the literature study, it was decided to make an EMS which uses ECMS and the dual decomposition method.

The modeled power flow of the system is shown in Figure 12. The symbols u_m and y_m are the input power and output power of each component m. The DC bus is represented by node n. The required power (i.e. the load power) is denoted by v.

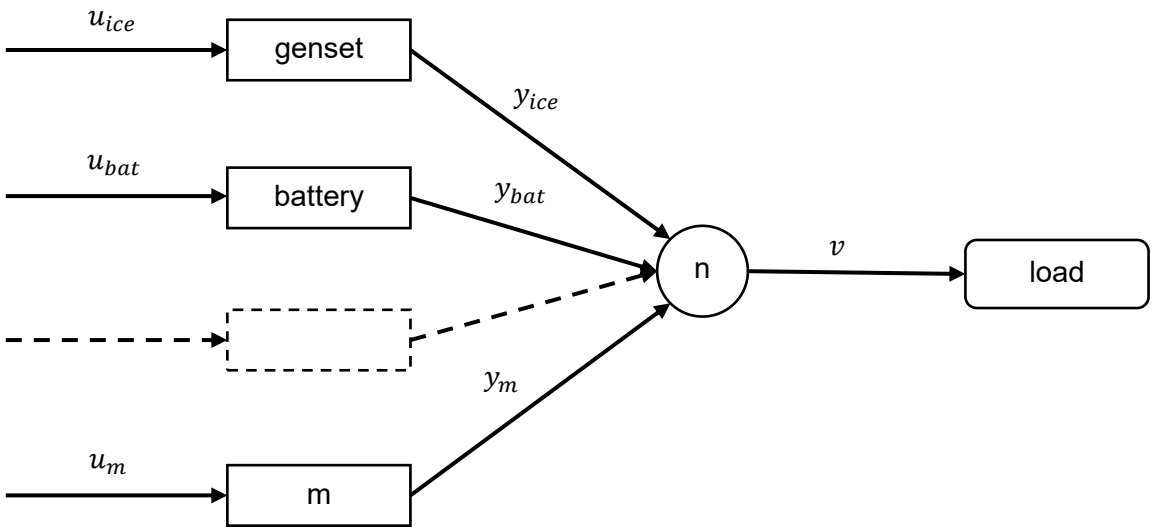

Figure 12 modeled power flow for a ship with electric propulsion

The EMS has two main goals: to satisfy the power balance (i.e. power supply has to match power demand) and to minimize fuel consumption. The power balance will be further explained in section 4.2. Minimizing fuel consumption is equivalent to minimizing the energy losses, as shown in [36]. This can be written as:

$$\min_{u_m(t),\, y_m(t)} \sum_m u_m(t) - y_m(t) \tag{1}$$

The relation between u_m and y_m is described by quadratic equality constraint (*2*):

$$y_m(t) + q_m\, u_m^2(t) + f_m\, u_m(t) + e_m = 0 \tag{2}$$

With $q_m(t)$, $f_m(t)$ and $e_m(t)$ being efficiency coefficients of module m, where $q_m > 0$. This makes sure the function shown in Figure 16 is continuous, with a positive derivative. These efficiency coefficients are time dependents, because the efficiency curve of a component can change over time. The power input is subject to:

$$u_{m,min}(t) \leq u_m(t) \leq u_{m,max}(t) \tag{3}$$

Where $u_{m,min}(t)$ and $u_{m,max}(t)$ are the minimum and maximum input power respectively of component m. To get coefficients $q_m(t)$, $f_m(t)$ and $e_m(t)$ for the gensets, a second order approximation of the power curves (Figure 9) was created using the least squares method. The

approximated power curves and corresponding efficiencies are shown with the dashed lines in Figure 13.

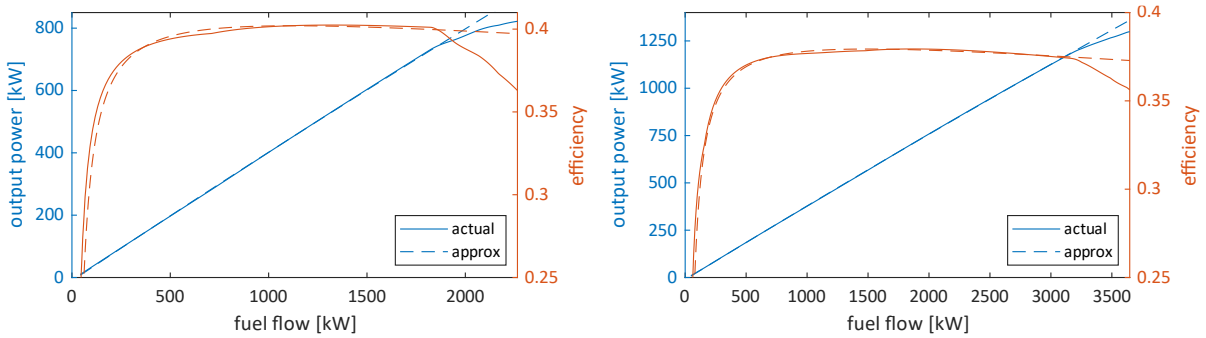

Figure 13 second order approximation of the power and efficiency curve for the LP genset (left) and HP genset (right)

4.1 Equivalent Consumption Minimization Strategy

ECMS works on the principle that a cost is assigned to the energy in the batteries or other ESS. This cost factor makes the cost of the stored energy equivalent to that of the quantity of fuel which would otherwise be used or saved [23]. Without this cost factor, minimizing objective function (*1*) would result in using only battery power, because a battery has lower energy losses compared to diesel gensets. For an EMS using ECMS, the objective function (*1*) is rewritten as:

$$\min_{u_m(t),\, y_m(t)} \sum_m \big(1 + \lambda_m(t)\big) * u_m(t) - \; y_m(t) \tag{4}$$

Where $\lambda_m(t)$ is the equivalent cost factor. The equivalent cost factor represents how 'expensive' the stored energy is. For non ESS components, such as gensets, the value of $\lambda_m(t)$ will be zero. For batteries this will be a positive value. A higher value of $\lambda_m(t)$ means the stored energy is worth more fuel per unit of energy.

In simple ECMS systems the equivalent cost factor is constant during the entire operating profile/driving cycle [23], [25]. This can lead to a near optimal solution with respect to an offline global optimization solution [37]. However, these results can only be obtained when the cost factor is specifically tuned for the system and operating profile. If the operating conditions are different than those for which the cost factor was tuned, it can easily lead to exceeding the allowed SoC boundaries [37]. Therefore, a constant equivalent cost factor is not suitable for an MPS EMS. This can be solved by using an adaptive equivalent cost factor. In [38] a proportional-integral controller based on the deviation from a reference SoC is used is to adjust the equivalent cost factor. However, this method requires tuning of the proportional and integral coefficients. This tuning requires knowledge of the operating profile and power train. Therefore, a different method for an adaptive equivalent cost factor was chosen for the MPS EMS [23], [39], which is described below.

4.1.1 Adaptive equivalent cost factor

If the energy in the battery was generated using the gensets in the system, that energy has cost a certain amount of fuel. The equivalent cost factor relates the amount of (fuel) energy spent to the amount of stored energy. Thus giving the stored energy a cost equivalent to using fuel. Gensets

will not always use the same amount of fuel to generate a certain amount of electrical energy, because fuel efficiency is not always the same. This is especially the case when different types of gensets are considered. The equivalent cost factor will depend on the (average) efficiency of the gensets [39], [40]:

$$\lambda_0 = \frac{1}{\eta_{avg}} - 1 = Q_{lhv} * BSFC_{avg} - 1 \tag{5}$$

Where λ_0 is the base value of the equivalent cost factor, relating the cost of electric energy to the fuel it cost to produce it. With:

$$BSFC_{avg} = \sum_{gensets} \frac{m_{fuel,m}}{E_{out,m}} \tag{6}$$

Where $m_{fuel,m}$ is the total fuel consumption of each genset and $E_{out,m}$ is the total energy output of each genset. To make sure the SoC does not go outside of its permitted range, an SoC-dependent penalty function can be introduced to the equivalent cost factor [23], [39]:

$$\lambda_m(t) = \lambda_0 * p(SoC_m(t)) \tag{7}$$

$$p(SoC_m(t)) = \begin{cases} 1 - p_f \left(\frac{SoC_m(t) - SoC_{ref}}{SoC_{max} - SoC_{ref}} \right)^a & for\ SoC_m(t) \geq SoC_{ref} \\ 1 - p_f \left(\frac{SoC_m(t) - SoC_{ref}}{SoC_{ref} - SoC_{min}} \right)^a & for\ SoC_m(t) < SoC_{ref} \end{cases} \tag{8}$$

Where a has a positive, odd integer value. The parameter p_f determines how far $p(SoC(t))$ will deviate from a value of 1 at the SoC limits. Figure 14 shows the results of equation (*8*) for different values of a. In this example, SoC_{ref} is smaller than the average of SoC_{min} and SoC_{max}. For higher values of a, the penalty function will have very little effect until the SoC comes close to the minimum or maximum allowed values.

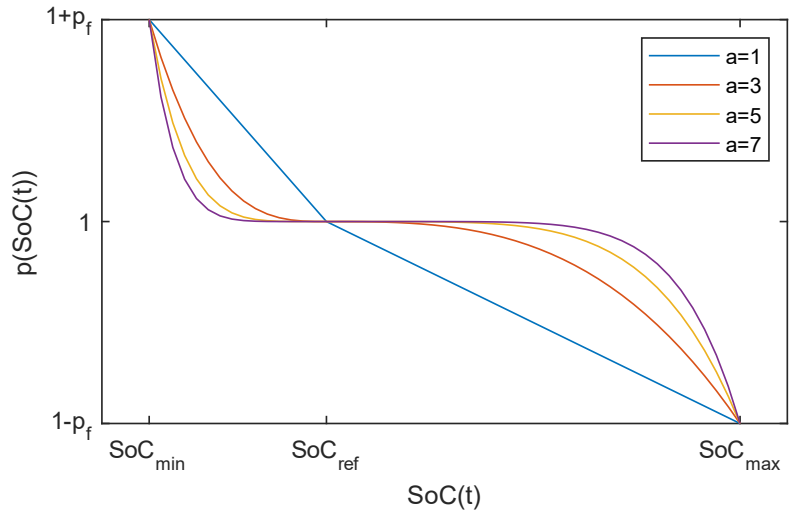

Figure 14 penalty function for the equivalent cost factor

4.2 Optimization algorithm

The optimization algorithm performs most of the calculations to determine the optimal power split, to satisfy equation (*4*). In this case the dual decomposition method is used, as explained in section 4.2.1. This method was chosen for the simplicity with which sub-problems (in this case: components) can be added [25], [36].

At node n the power balance needs to be satisfied. The balance equation is given by:

$$\Psi\, v(t) + \sum_m (\Gamma_m u_m(t) + \Phi_m y_m(t)) = 0 \tag{9}$$

Where Ψ, Γ and Φ are connectivity matrices which connect the balance equations of different nodes. Because the considered electric propulsion system only has one node (the DC bus), these matrices are 1x1. Because all modules connect to the node in the same way, the connectivity matrices are the same for all components:

$$\Psi = 1 \quad \Gamma_m = 0 \quad \Phi_m = -1$$

Therefore, for the considered electric propulsion system, the balance equation (*9*) can be simplified to:

$$v(t) - \sum_m y_m(t) = 0 \tag{10}$$

4.2.1 Dual decomposition

Dual decomposition has been used for large scale optimization problems since the early 1960s [41]. It is a mathematical method where the coupling between sub-problems is relaxed using Lagrange multipliers [42].

The optimal control problem (*4*) is decomposed by introducing a partial Lagrangian [25]. A Lagrange equation consists of two parts: a function for which a minimum (or maximum) needs to be found (in this case: objective function (*4*)) and a constraint (in this case: balance equation (*9*)) which is multiplied by a Lagrange multiplier:

$$L\big(\{u_m(t),\, y_m(t)\}_m, \mu(t)\big) = \left(\sum_m (1+\lambda_m) u_m(t) - y_m(t)\right) + \mu(t) * \left(v(t) - \sum_m y_m(t)\right) \tag{11}$$

Where $\mu(t)$ is the Lagrange multiplier related to the power balance at the node. This multiplier could be interpreted as a market price for energy, with the individual components being traders who want to maximize their profit. A higher market price means the individual components can earn more, even at lower profit margins (i.e. a higher power output, but with a lower efficiency). Then a market price can be found where supply matches demand. The partial Lagrange dual function of the optimal control problem is given by:

$$g(\mu(t)) = \min_{\{u_m(t),\, y_m(t)\}_m} L\big(\{u_m(t),\, y_m(t)\}_m, \mu(t)\big) \tag{12}$$

Solving (*12*) will give values for $u_m(t)$, $y_m(t)$, and $\mu(t)$ so that the objective function is minimized, and the balance equation is satisfied.

In (*12*) it holds that:

$$g(\mu(t)) = \mu(t)v(t) + \sum_m g_m(\mu(t)) \tag{13}$$

With:

$$g_m(\mu(t)) = \min\ (1 + \lambda_m)\, u_m(t) - \big(1 + \mu(t)\big)\, y_m(t) \tag{14}$$

Each of the Lagrange dual functions $g_m(\mu(t))$ is related to only one of the components, meaning that they can be solved independently. Because u_m and y_m are related to each other by (*2*), an analytical solution exists for (*14*). After substituting (*2*) into y_m, the only remaining variable is u_m. The solution of (*14*) for a given value of $\mu(t)$ can be found by solving the partial derivative:

$$\frac{\partial g_m(\mu(t))}{\partial u_m(t)} = 0 \tag{15}$$

The solution is given by:

$$u_m(t) = -\left(\frac{1+\lambda_m}{1+\mu(t)} + f_m\right)/2q_m \tag{16}$$

While still subject to (*3*).

Equation (16) can be substituted into (2) to obtain $y_m(t)$. Both $u_m(t)$ and $y_m(t)$ are now expressed as functions of $\mu(t)$. Therefore, $\sum_m\ y_m(t)$ can be expressed as a function of $\mu(t)$. Figure 15 shows an example for $y_m(t)$ as a function of $\mu(t)$ for individual components. The fact that the power output of every individual component can be expressed as a function of the same variable, means it is possible to add, remove, or change components, without influencing other components. Only the value of $\mu(t)$ for which the power balance (*10*) is satisfied will change.

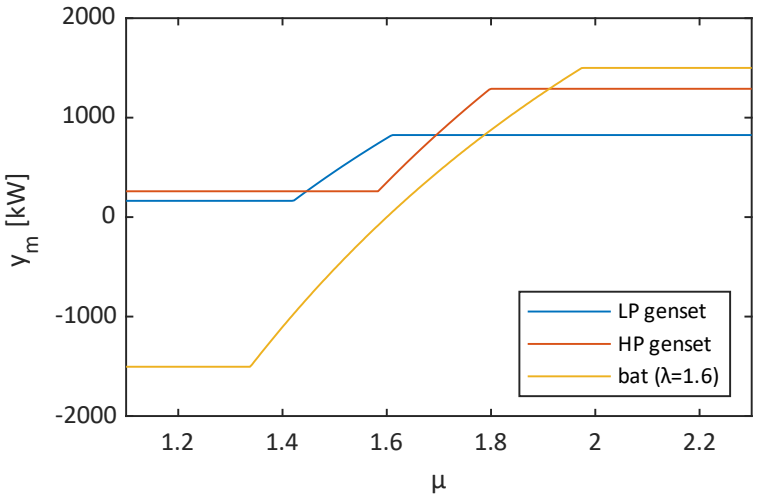

Figure 15 output power of different components as a function of μ

Figure 16 shows $\sum_m y_m(t)$ as a function of $\mu(t)$, for a configuration where one of each of the components shown in Figure 15 is used. It is important to note that these curves can change over time, as the efficiency curves of the components change. For example, the efficiency of a battery changes with SoC. Therefore, it is not possible to create a single look-up table which can be used during the entire simulation.

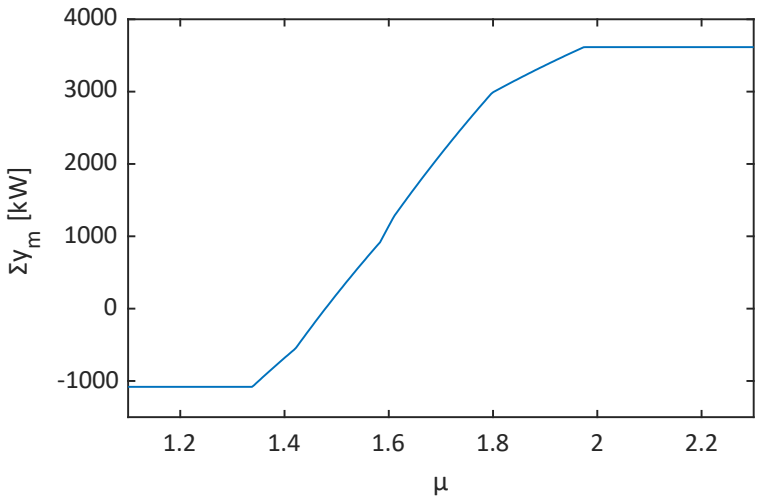

Figure 16 combined output power as a function of μ, for a configuration with one LP genset, HP genset and battery

If the required power $v(t)$ is within the range of $\sum_m y_m(t)$, there exists one value for $\mu(t)$ where power balance (10) is satisfied. It is important to note that this is only true if the relation between $u_m(t)$ and $y_m(t)$ is convex [42]. Otherwise, the curve as shown in Figure 16 could have a negative and/or infinitely steep slope, resulting in either zero of multiple possible values for $\mu(t)$. To calculate the entire curve as shown in Figure 16 for every timestep is very computationally expensive. Therefore, to find this value of $\mu(t)$, the steepest ascend method is used. This is an iterative approach, where at each iteration s the dual function (14) is minimized for each module. This is followed by an update of the dual variable:

$$\mu^{s+1}(t) = \mu^s(t) + \alpha^s \left(v(t) - \sum_m y_m^s(t) \right) \tag{17}$$

Where α^s is a suitably chosen value for the step size. Iterating will continue until a convergence criterium ε is reached, or a predetermined maximum number of iterations s_{max} is reached. ε is the amount of power the solution is allowed to deviate from satisfying the power balance (*10*). The used divergence criterium is:

$$\left| v(t) - \sum_m y_m^s(t) \right| < \varepsilon \tag{18}$$

When the convergence criterium is reached, a value for $\mu(t)$ is found where the solution of (14) mostly satisfies the power balance. There will be a small difference between the required power and the power output found by the EMS, of between 0 and ε. This difference will be compensated for by the batteries.

When two or more identical components are used (for example, two LP gensets), equation (16) will give the same output for all of them. This means the EMS will ask the same power output from each.

4.2.2 Effect of the equivalent cost factor on the dual function

As shown in Figure 17, the value of λ_m shifts the range where μ will affect y_{bat}. This, in turn, will affect at what value of μ equation (*17*) will converge for the required power output. This is illustrated in Figure 18 for a required power of 1700 kW.

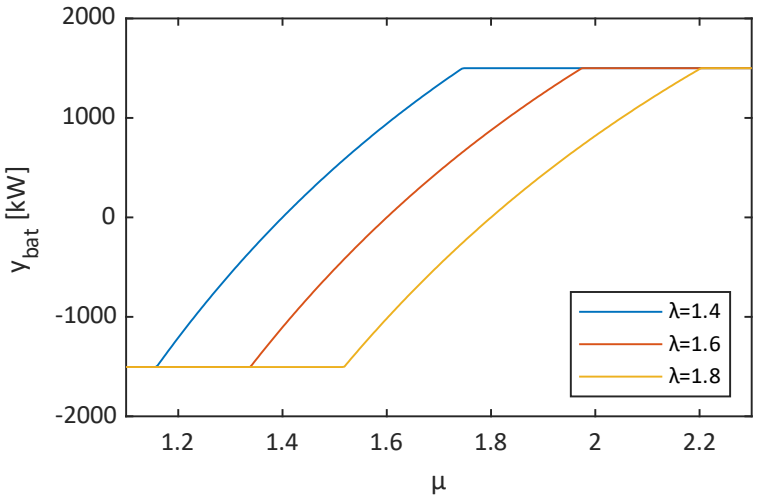

Figure 17 battery power as a function of μ, for different values of the equivalent cost factor λ

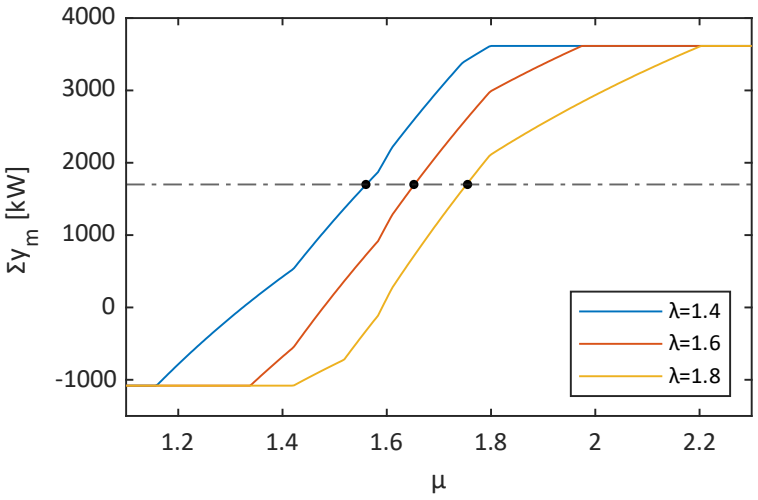

Figure 18 combined output power for different values of λ, for a configuration with one LP genset, HP genset and battery. The black dots indicate where equation (17) will converge for the different values of λ, for a required power of 1700 kW

Table 5 shows at which value of $\mu(t)$ equation (17) converges when the required power is 1700 kW, as well as the corresponding power split (when considering one LP genset, one HP genset, and one battery). 1700 kW is half of the required power of 'fast cruising', but only half of the installed components of configuration 1 (Table 4) are used here. This also illustrates how the power split will lean more towards battery power when the equivalent cost factor is lower.

Table 5 power split for different values of λ

λ	μ at 1.7 MW	LP genset [kW]	HP genset [kW]	Battery [kW]
1.4	1.56	661.0	259.7	779.3
1.6	1.65	825.0	614.6	260.4
1.8	1.75	825.0	1090.0	-215.0

4.2.3 Initial value for the dual variable

For equation (*17*) an initial value is needed for the dual variable: $\mu^0(t)$. Ideally, this value is as close to the desired value of $\mu(t)$ as possible. When equation (*17*) has converged during the previous timestep, it can be assumed that $\mu(t_{previous})$ is close to this desired value, in the case that required power and SoC do not change significantly. In this case:

$$\mu^0(t) = \mu(t_{previous}) \tag{19}$$

However, if the previous timestep did not converge, a new value will need to be chosen for $\mu^0(t)$. The value halfway between $\mu_{min}(t)$ and $\mu_{max}(t)$ was chosen for this. $\mu_{min}(t)$ and $\mu_{max}(t)$ represent the outer values where $\mu(t)$ affects $\sum_m y_m(t)$, as shown in Figure 16. These values can be found by first solving (*16*) for $\mu(t)$:

$$\mu(t) = -\frac{1 + \lambda_m(t)}{2q_m * u_m(t) - f_m} - 1 \tag{20}$$

And then finding the outermost values for any of the connected components using (*3*):

$$\mu_{max}(t) = \max_m -\frac{1 + \lambda_m(t)}{2q_m * u_{m,max}(t) - f_m} - 1 \tag{21}$$

$$\mu_{min}(t) = \min_m -\frac{1 + \lambda_m(t)}{2q_m * u_{m,min}(t) - f_m} - 1 \tag{22}$$

Where $u_{m,max}(t)$ and $u_{m,min}(t)$ are determined by the modules. Now $\mu^0(t)$ becomes:

$$\mu^0(t) = \frac{\mu_{max}(t) + \mu_{min}(t)}{2} \tag{23}$$

4.2.4 Step size for the steepest ascend method

Equation (*17*) needs to converge to reach the convergence criterium. How many iterations are needed for this depends on the value of the step size α^s. When the step size is very small, many iterations are needed, which will cost more computational energy. Therefore it is desirable to choose a larger step size. However, equation (*17*) will become unstable when α^s is too large. The 'ideal' step size depends on $\mu_{max}(t)$, $\mu_{min}(t)$, and the range of $\sum_m y_m(t)$, i.e. the slope and range of a curve as shown in Figure 16. This means it is not possible to choose a single value for α^s, which works for all configurations. In [36], [43] it is proposed to use a Newton scheme to determine the step size. This is derived as follows:

Equation (*17*) is fully converged when $\mu^{s+1}(t) = \mu^s(t)$. For $\alpha^s \neq 0$, this is the case when:

$$v(t) - \sum_m y_m^{s+1}(t) = 0 \tag{24}$$

The value for y_m^{s+1} can be approximated linearly:

$$y_m^{s+1} \approx y_m^s + \frac{\partial y_m^s}{\partial \mu}(\mu^{s+1} - \mu^s) \tag{25}$$

When substituting (*25*) into (*24*) and solving for $\mu^{s+1}(t)$, we get:

$$\mu^{s+1}(t) = \mu^s(t) + \left(-\sum_m \frac{\partial y_m^s}{\partial \mu}\right)^{-1} * \left(v(t) - \sum_m y_m^s(t)\right) \tag{26}$$

This is the same as (*17*) with:

$$\alpha^s = \left(-\sum_m \frac{\partial y_m^s}{\partial \mu}\right)^{-1} \tag{27}$$

After substituting (*16*) into (*2*), the analytical solution for this is:

$$\alpha^s = \left(\sum_m \frac{1}{2q_m} \frac{(\lambda_m(t)+1)^2}{(\mu^s(t)+1)^3}\right)^{-1} \tag{28}$$

Using this method, the convergence criterium was always reached within seven iterations, for the tested configurations and operating profiles.

4.3 Implementation

The methods mentioned previously in this chapter are implemented in the MPS EMS. To solve the power split, the EMS needs to know the properties of the installed components. These properties are: maximum power output (P_{max}), minimum and maximum power output for the next time-step ($P_{min}(t)$, $P_{max}(t)$), which could be limited by ramp rates, equivalent cost factor ($\lambda(t)$), coefficients for the quadratic power curve (q(t), f(t), e(t)), and a penalty for switching a component on (on/off penalty). These properties are communicated to the EMS by each component individually. These properties can have a value of zero for certain components (e.g. the cost factor for the gensets). Using this data, the EMS will determine the desired power output of each of the components, as well as which components should be switched on or off, as shown in Figure 19. The base value of the equivalent cost factor, λ_0, is calculated separately. Because the power split has to be computed, it can not be updated continuously, but is instead updated at discrete timesteps. The EMS will determine the power split once every timestep τ. For simulations τ needs to be equal to, or larger than the simulation timestep.

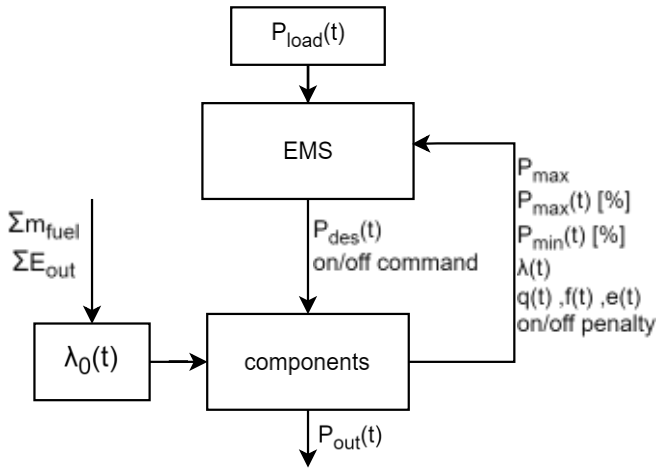

Figure 19 diagram showing the exchange of data in the system

Within the EMS various steps are taken to come to the desired power split, as shown in Figure 20. First, it is determined which configurations, in terms of which components are switched on or off, are viable. This is done to prevent spending computational power on configurations that are unable to satisfy the power balance. The amount of possible configurations is:

$$n_{config} = 2^N - 1 \tag{29}$$

Where N is the number of installed components. For six components this gives 63 possible combinations. A list is made which counts from 1 to $n_{config} + 1$ in binary, where each digit represents the on/off state of one of the installed components, as illustrated below for configuration 1 (Table 4):

LP gen 1	LP gen 2	HP gen 1	HP gen 2	Bat 1	Bat 2
0	0	0	0	0	1
0	0	0	0	1	0
0	0	0	0	1	1
			⋮		
1	1	1	1	0	1
1	1	1	1	1	0
1	1	1	1	1	1

Because turning off batteries does not have advantages, they are assumed to be always on. This reduces the number of unique combinations to 16. If a component has failed, all configurations where it is used are disregarded. For each of the remaining configurations, the maximum combined power output is calculated. If this is lower than $P_{load}(t)$ the configuration is non-viable for the coming timestep. Then, μ_0 is calculated for each remaining configuration using (*23*).

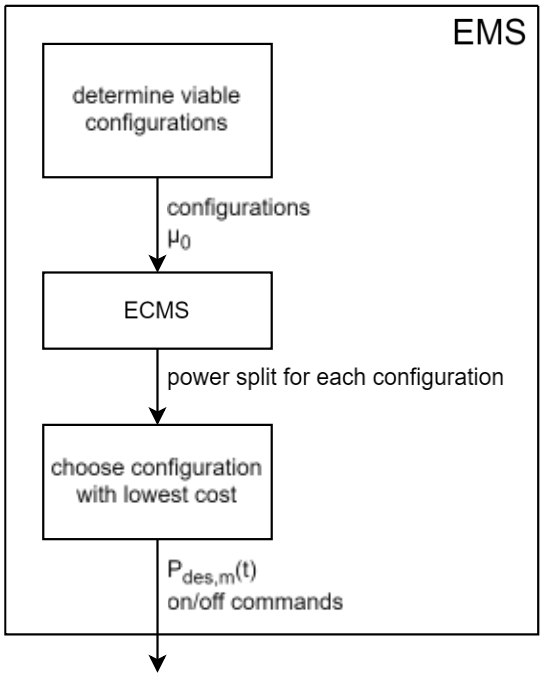

Figure 20 diagram showing order of operations of the EMS

Then the ideal power split, according to ECMS, is calculated using the dual decomposition method as described in section 4.2.1. This process is depicted in Figure 21. The ideal power split is calculated for each of the predetermined viable configurations separately.

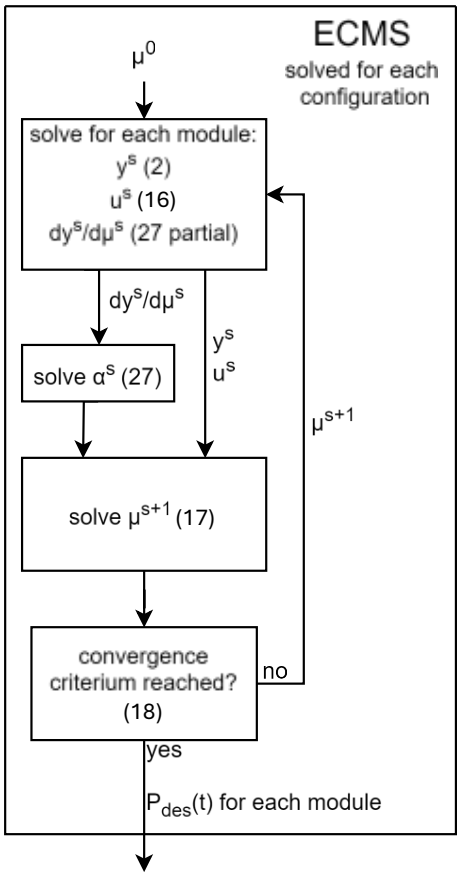

Figure 21 diagram showing iterative process of the ECMS using dual decomposition, with equation numbers

To prevent frequent on/off switching of components, a penalty for switching on components is added to the objective function (*4*) [38]. This penalty is determined per component, and is only applied when that component would need to be switched on for the configuration currently being evaluated. The value of this penalty is zero for the batteries, as it does not cost any additional energy to switch them on or off. For the gensets, ideally this would depend on the additional fuel cost of switching them on. As this was unknown, the value for the penalty was set to a percentage of the genset's maximum output.

$$\min_{u_m(t),\, y_m(t)} \sum_m (1 + \lambda_m(t))u_m(t) + y_m(t) + penalty_m \tag{30}$$

The last step in the EMS is to choose the configuration which best satisfies objective function (*30*). Using the power split as determined by the ECMS, equation (*30*) is evaluated for each of the viable configurations. Then the configuration with the lowest value for (*30*) is chosen as the best option. If multiple configurations have the exact same value, the one furthest down in the list will be selected. The corresponding desired power outputs are then communicated to the components.

4.4 Benchmark systems

To show the developed EMS is not only capable of dealing with an MPS, but can also provide good fuel economy, two benchmark systems are used: a global optimization, and an RB EMS (section 4.4.2).

4.4.1 Global optimization benchmark

The global optimization used as a benchmark in this thesis, is an adapted version from the one used in [40]. The on/off switching, the running time and the corresponding power of the components are scheduled using the MILP algorithm.

For the gensets the power output as a function of power input is modeled linearly. Because the actual curves have a clear point where efficiency starts to decrease, a piecewise linear approximation is applied to improve accuracy. Two separate linear approximations were done for different power output ranges of each genset. The resulting power and efficiency approximations are shown in Figure 22. The battery model is simplified to have a constant efficiency, regardless of SoC or (dis)charge rate. The objective function of the used global optimization method is to minimize the genset fuel consumption over the entire voyage.

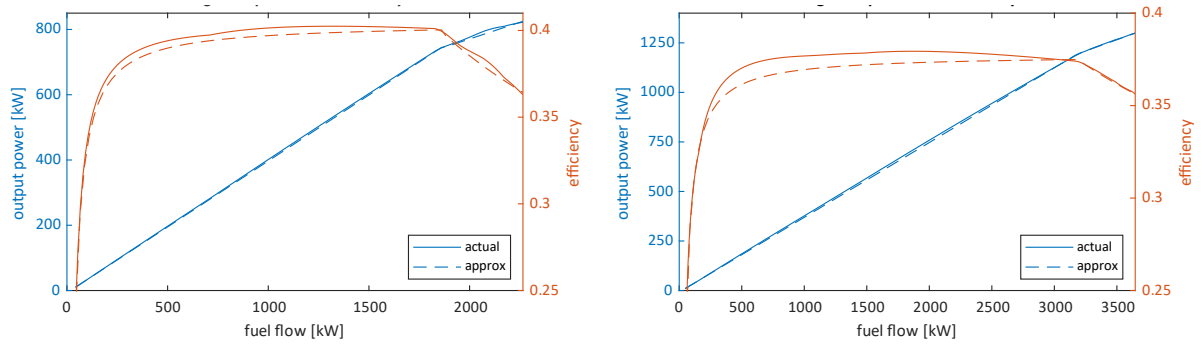

Figure 22 optimal power and efficiency curve for the LP genset (left) and HP genset (right), with a piecewise linear approximation

The global optimization gives the desired power output of each of the gensets. This data is then used to run a simulation using the actual component models. The results of this simulation is used as a benchmark for the MPS EMS.

As a consequence of the simplified battery model, the actual SoC will slightly diverge from the calculated SoC, as the simulation goes on. This made it unfeasible to use this method for the longer operating profile, as the SoC would exceed the set limits.

4.4.2 RB EMS benchmark

An RB EMS was made for each of the four tested configurations. Because RB EMS only work with a specific power plant configuration, three different RB EMS needed to be made. Battery capacity is not taken into account by these EMS, only SoC. Therefore, configuration 1 and 3 can use the same RB EMS. These RB EMS are based on the charge depleting/charge sustaining (CD/CS) principle. A typical CD/CS EMS will start by only using battery power until the minimum allowed SoC is reached, after which it will switch to engine power and keep the battery SoC in a very narrow range [29].

Because using only battery power would drain the batteries within a few hours, gensets will also be used in CD mode. While in CD mode, the gensets will be limited to a power range where they are most fuel efficient. For the LP genset this range was set to 350-750 kW. For the HP genset this range was set to 600-1000 kW. For configuration 4 these values are doubled, since the gensets have double the power.

When the SoC drops below 40%, the system will switch to CS mode. In this mode all power will be provided by the gensets. When the required power exceeds the efficient operating range of a genset, the next genset will be activated. During very high power demand the gensets will need to exceed their efficient operating range.

For the configurations where both types of gensets are used (1, 3 and 4) the LP gensets will be activated before the HP gensets, because of their higher fuel efficiency.

5 Results and discussion

In this chapter the performance of the developed EMS will be shown and discussed. Firstly, it is discussed how the performance will be assessed. Then, the simulation set-up will be elaborated upon. And finally, the simulation results will be shown and discussed.

5.1 Assessment methods

The goal of this thesis is to develop an EMS which can handle an MPS, while minimizing fuel consumption. To assess the performance for minimizing fuel consumption, the developed EMS is compared to other methods: an RB EMS using the CD/CS principle (section 4.4.2), and a global optimization using a MILP algorithm (section 4.4). The global optimization was only done for operating profile 1, because the SoC during the simulation does not exactly follow the SoC expected by the global optimization. This is caused by the simplified battery model used by the global optimization. The discrepancy between the expected SoC and the actual SoC increases with time, which would cause the SoC to go outside of its allowed limits during operating profile 2

To show the developed EMS can handle an MPS, it is tested with four different configurations (Table 4), and two different operating profiles (Figure 6 and 7). All tests are performed without manually changing any control parameters, i.e. the EMS was not adjusted to better suit individual configurations or operating profiles.

It is also important that the EMS can handle the hardware configuration changing during a voyage. One scenario where this happens, is when a component fails and has to be shut off for the rest of the voyage. If an RB EMS were subjected to such a scenario, it would only be able to keep operating reliably if the specific failure was accounted for during development. The performance of the MPS EMS in such a scenario was tested by disabling one of the components during the voyage.

5.2 Simulation set-up

Only two things are altered between simulations: the operating profile and the hardware configuration. The value of some control parameters needs to be chosen manually, but these values do not need to be altered for different operating profiles and hardware configurations. The chosen values for these parameters are shown in Table 6. The simulation timestep was set to 0.1 seconds. All simulations were run using MATLAB Simulink (version R2022b), on a desktop pc with an AMD Ryzen 7 3700X processor (release date: 2019). The simulations took around 4 minutes for operating profile 1, and around 38 minutes for operating profile 2. This shows the speed of the controller, as well as the real-time applicability.

Table 6 control parameters used during simulations

Parameters	Value
$\boldsymbol{\tau}$	10 [s]
$\boldsymbol{\varepsilon}$	1 [kW]
$\boldsymbol{SoC_{ref}}$	70 [%]
$\boldsymbol{a}$	3
$\boldsymbol{p_f}$	0.3
$\boldsymbol{\lambda_0(t=0)}$	1.55

The parameter values for the FMUs of the batteries and gensets are shown in Table 7 and 8 respectively. With the exception of battery capacity for hardware configuration 3, all FMU parameters were kept as provided by TNO.

Table 7 parameters used during simulations for each battery FMU

Parameters	Battery
Nominal capacity [Ah]	5000 (10000 for config 3)
Nominal voltage [V]	805
Initial SoC [%]	70
Upper bound SoC [%]	95
Lower bound SoC [%]	35

Table 8 parameters used during simulations for each genset FMU

Parameters	LP genset	HP genset
Inertia of the engine [kg m^2]	14.0	22.0
Inertia of the electric motor [kg m^2]	0.007	0.007
Rated efficiency of the electric motor [%]	97	97
P action for the speed control [-]	0.064	0.064
I action for the speed control [-]	0.16	0.16

5.3 Simulation results

For each operating profile and hardware configuration, three graphs are shown: power output per component, active gensets, and SoC. Because the batteries have identical properties, as well as the same starting SoC, their SoC remains identical. For hardware configuration 1, 2 and 3 these graphs will also be shown for the benchmarks. Fuel consumption is shown in Table 9.

The results for operating profile 1 will be discussed first, for both the developed EMS and the benchmarks. This is followed by the results for operating profile 2. Then fuel consumption is shown and compared to the benchmarks. Lastly, the results for when a component fails are discussed, including fuel consumption.

5.3.1 Operating profile 1

Firstly, the developed EMS was able to control all tested hardware configurations, while keeping all components within their operating limits, and maintaining the balance between required power and generated power (Figure 23-26).

It can be observed that the batteries are discharged during high and very high power demand, while being charged during low and medium power demand. This behavior is less pronounced for configuration 2.

It is also observed that during charging of the batteries, while power demand is low, the charging power slowly decreases, until the genset is turned off. This happens because the equivalent cost factor changes (through equation (7) and (8)) as the SoC gets closer to the SoC limit.

For configuration 1, 3, and 4 it is observed that the HP gensets will only be switched on when power demand is high. The LP gensets are even ramped up to full power before a HP genset is used. This is as expected, because the approximated efficiency (Figure 9) of the LP genset is

higher than that of the HP genset. However, if the actual efficiency curves were used, the HP genset(s) would be activated sooner, due to the efficiency drop-off of the LP genset at high power. This would likely result in a slightly lower overall fuel consumption.

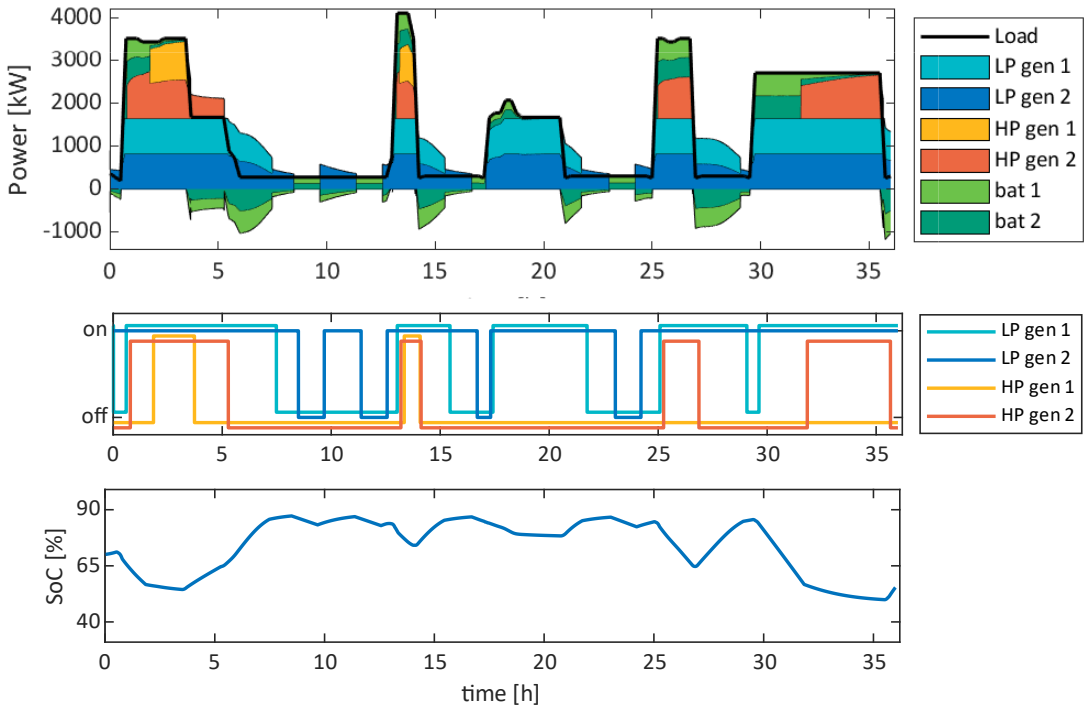

Figure 23 simulation results for hardware configuration 1, and OP 1

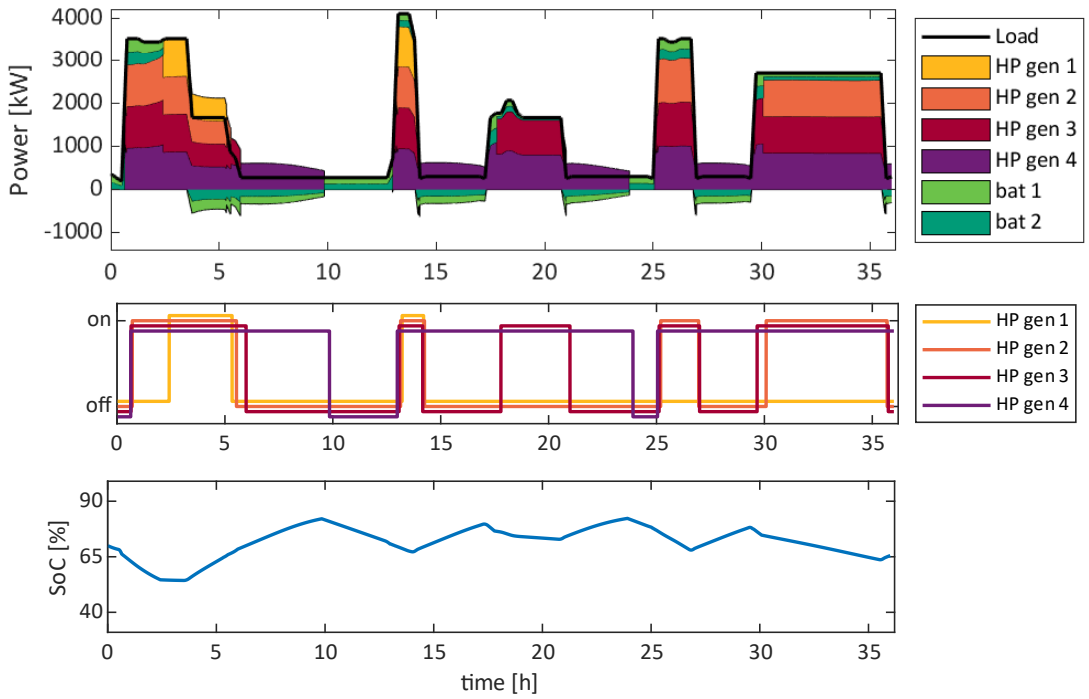

Figure 24 simulation results for hardware configuration 2, and OP 1

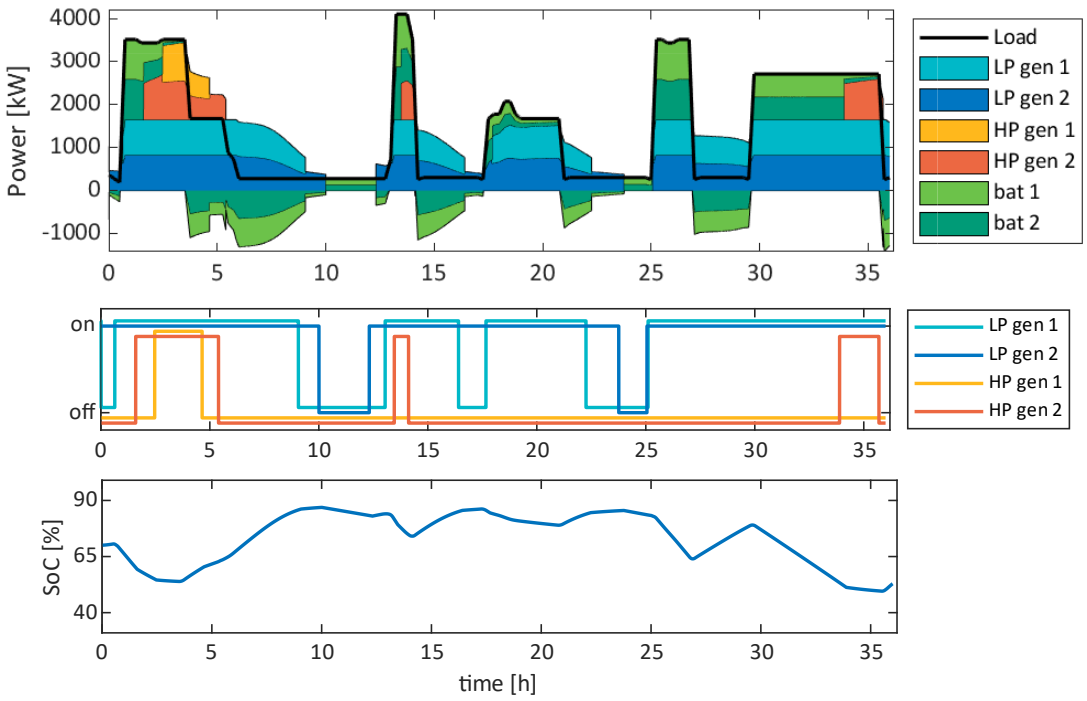

Figure 25 simulation results for hardware configuration 3, and OP 1

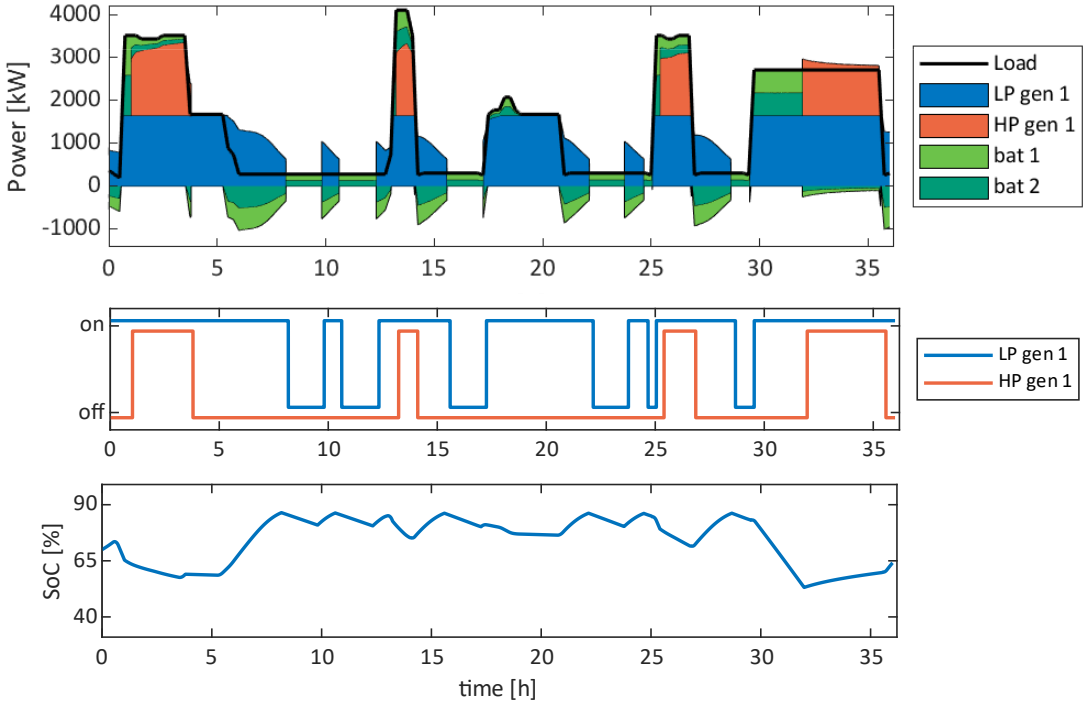

Figure 26 simulation results for hardware configuration 4, and OP 1

5.3.1.1 Global optimization

The simulation results for the global optimization, for configuration 1 and operating profile 1 are shown in Figure 27. The results for the other configurations can be found in appendix B.

It is immediately clear the global optimization makes more use of the batteries than the other EMSs. This is partly caused by the fact that the global optimization assumes a constant battery efficiency, regardless of SoC or (dis)charge rate.

The largest reason for the intensive use of the batteries is the minimization of the use of the less efficient HP gensets. This effect is even more pronounced for configuration 3. This is why the batteries are used far less with configuration 2, where all installed gensets are identical.

Another behavior that reduces fuel consumption, is that the gensets are never used at maximum power. Using the piecewise linear approximation (as shown in Figure 22), the most efficient operating point seems to be at the point where the two piecewise approximations meet. This is the point where the gensets are operated mostly by the global optimization.

One important to note is that the global optimization only minimizes genset fuel consumption. As a result it aims to have the final SoC equal to the lower bound SoC limit. Furthermore, there is no penalty for switching the gensets on or off. As a consequence, gensets will sometimes be switched on or off very briefly.

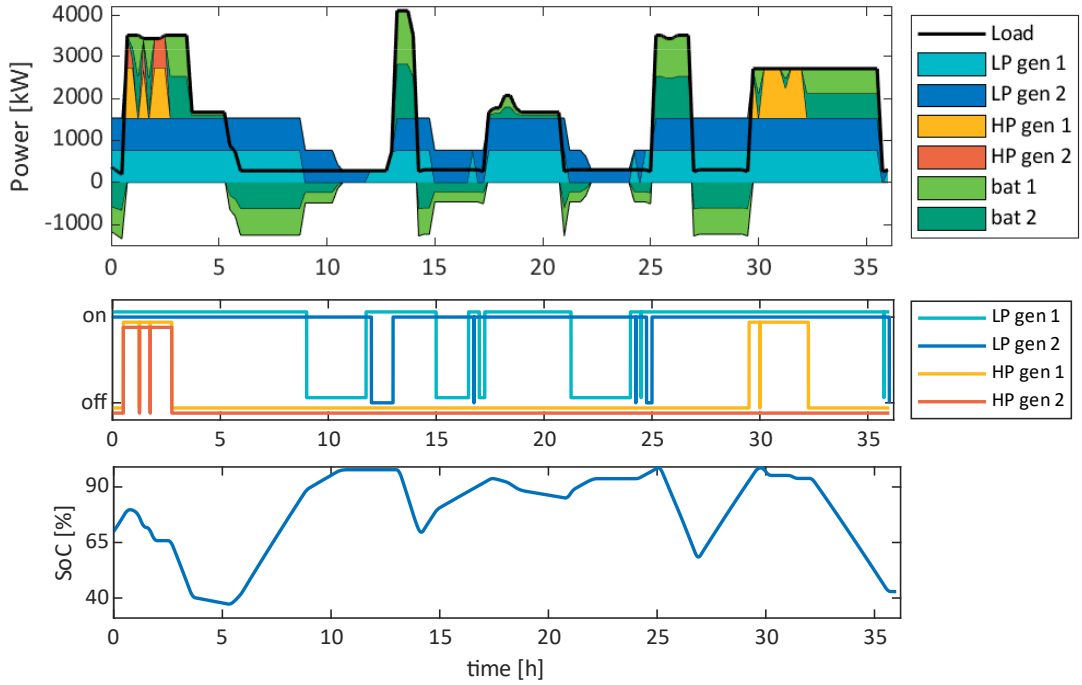

Figure 27 simulation results for hardware configuration 1, and OP 1, with the global optimization

5.3.1.2 RB EMS

The simulation results for the RB EMS, for configuration 1 and operating profile 1 are shown in Figure 28. The results for the other configurations can be found in appendix A.

Because the RB EMS uses the CD/CS principle, the batteries are never recharged (i.e. battery power will not go below zero). It is observed that battery power is only used at low and very high power demand, while in CD mode. This is because at medium to high power demand, the gensets can run at an efficient operating point (as determined in section 4.4.2).

The downside of the CD/CS strategy, combined with this hardware configuration and operating profile, is that the batteries reach their minimum SoC long before the end of the voyage. This means that during low power demand, one of the gensets will have to run at low power, where it has relatively low fuel efficiency.

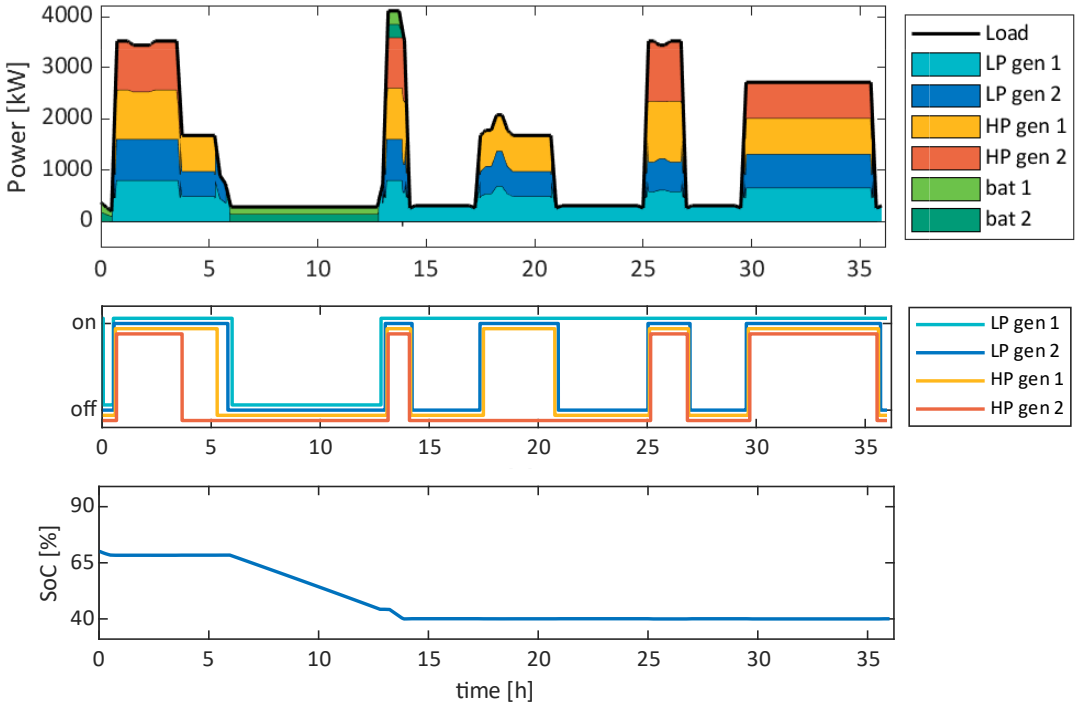

Figure 28 simulation results for hardware configuration 1, and OP 1, with the RB EMS

5.3.2 Operating profile 2

As with operating profile 1, the developed EMS was able to control all tested hardware configurations, while keeping all components within their operating limits, and maintaining the balance between required power and delivered power. This shows the EMS can work for operating profiles of different length and power requirements.

It is observed that the SoC reaches different levels of equilibrium for different levels of required power. When required power is high the batteries are drained, which causes equation (8) to increase the equivalent cost factor. At some point the ECMS will prefer increasing genset power, or the amount of active gensets. When the required power goes down to a medium level, the inverse happens. During operating profile 1 the length of time remaining at a certain required power level is significantly shorter. Therefore, this behavior is not as obvious for operating profile 1.

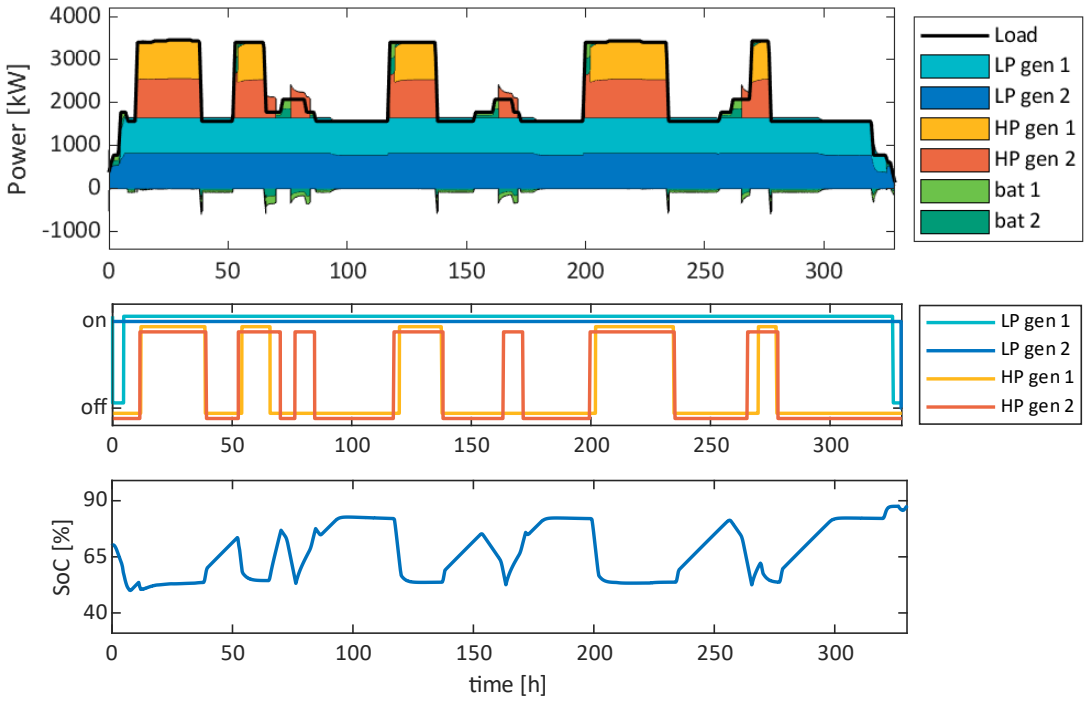

Figure 29 simulation results for hardware configuration 1, and OP 2

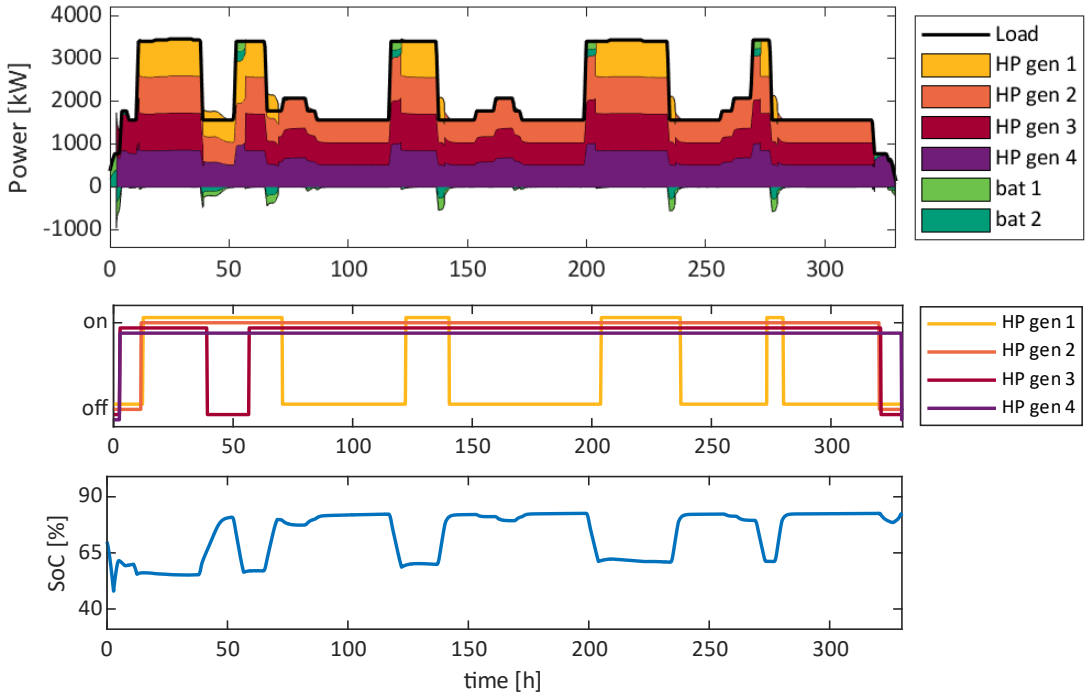

Figure 30 simulation results for hardware configuration 2, and OP 2

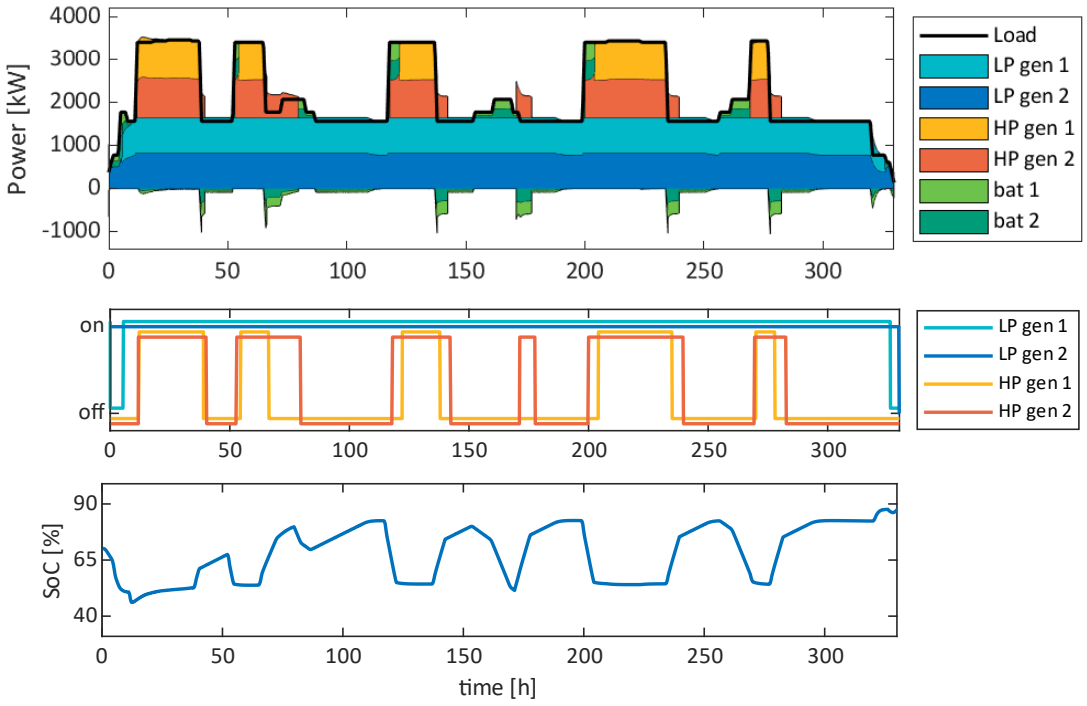

Figure 31 simulation results for hardware configuration 3, and OP 2

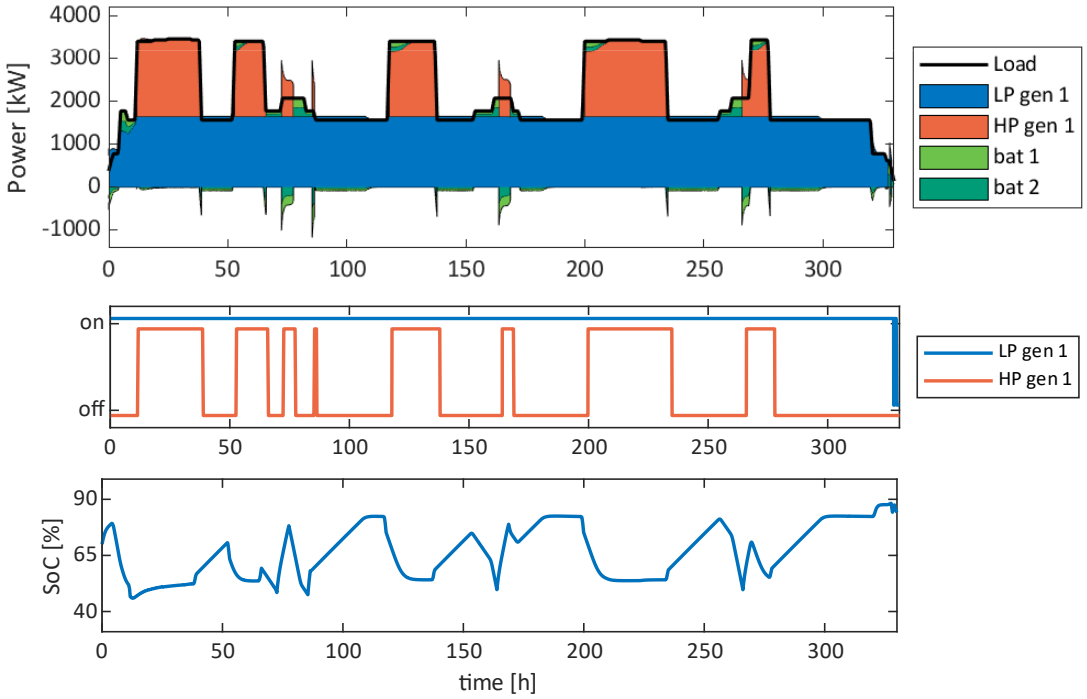

Figure 32 simulation results for hardware configuration 4, and OP 2

5.3.2.1 RB EMS

The simulation results for the RB EMS, for configuration 1 and operating profile 2 are shown in Figure 33. The results for the other configurations can be found in appendix A.

As with operating profile 1, battery power is only used at low and very high power demand, while in CD mode. However, because the power demand of operating profile 2 is almost exclusively between medium and high power, the batteries are not used during the majority of the voyage. The battery SoC never gets low enough for the RB EMS to switch to CS mode. This means the gensets can run at fuel efficient operating points for the entire voyage. Another consequence is that having larger batteries (configuration 3) does not affect fuel consumption.

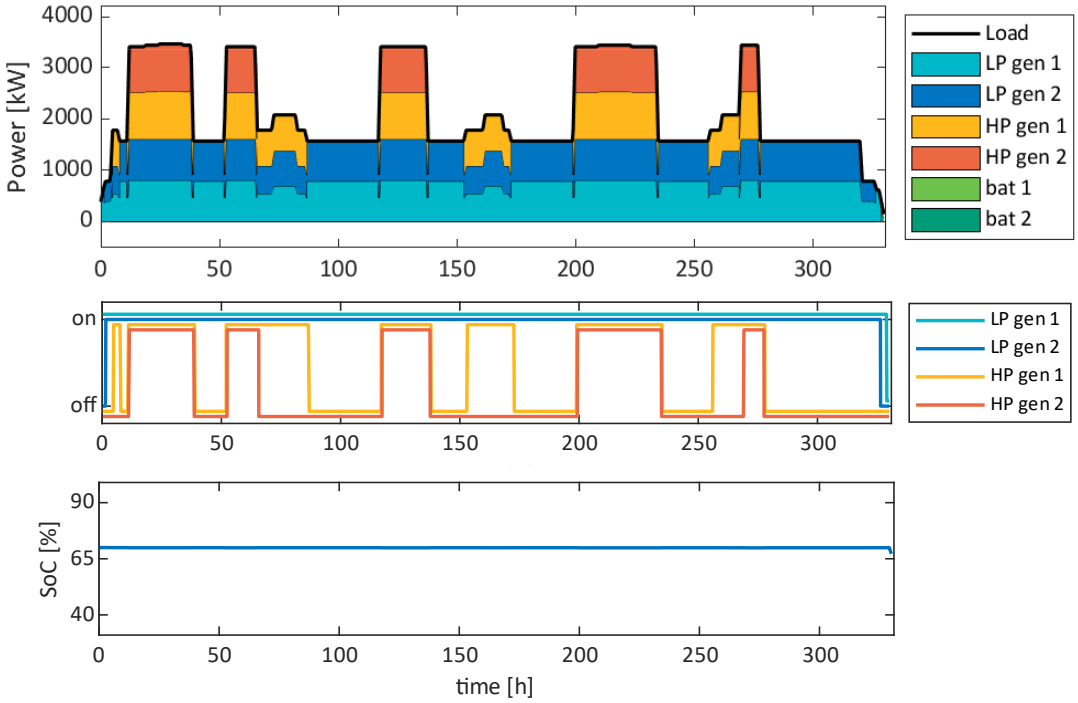

Figure 33 simulation results for hardware configuration 1, and OP 2, with the RB EMS

5.3.3 Fuel consumption

The fuel consumption, and corrected fuel consumption, of all simulations can be found in Table 9. The corrected fuel consumption, $m_{fuel,cor}$, is calculated using equation (*31*), to account for the difference between initial SoC and final SoC. This is done because the MPS EMS, contrary to the benchmark systems, will not try to drain the batteries before the end of the voyage. Therefore, the fuel which was saved (or used) by discharging (or charging) the batteries is added to the actual fuel consumption.

$$m_{fuel,cor} = m_{fuel} + \Delta SoC * C_{bat} * \frac{\lambda_0 + 1}{Q_{lhv}} \tag{31}$$

Where C_{bat} is the total battery capacity and ΔSoC the difference between the initial SoC and final SoC.

Figure 34 gives a visual representation of the corrected fuel consumption for all simulations. Figure 35 shows the corrected fuel consumption of the developed EMS relative to the benchmark

EMSs. A negative value means the benchmark has a lower corrected fuel consumption than the developed EMS.

Table 9 Fuel consumption [kg] and fuel consumption corrected for battery usage [kg] of the different hardware configurations for all OP, for both the proposed EMS and the benchmark systems

		Modular		**RB**		**Global**	
OP	**Config**	Fuel	Cor. fuel	Fuel	Cor. fuel	Fuel	Cor. fuel
1	1	10607	10855	10260	10766	10162	10613
1	2	10980	11057	10570	11092	10527	11145
1	3	10206	10780	9770	10784	9564	10569
1	4	10803	10903	10342	10854	10257	10663
2	1	151530	151240	148210	148260	-	-
2	2	154120	153920	152150	152280	-	-
2	3	152040	151460	148210	148260	-	-
2	4	151690	151450	149860	150370	-	-

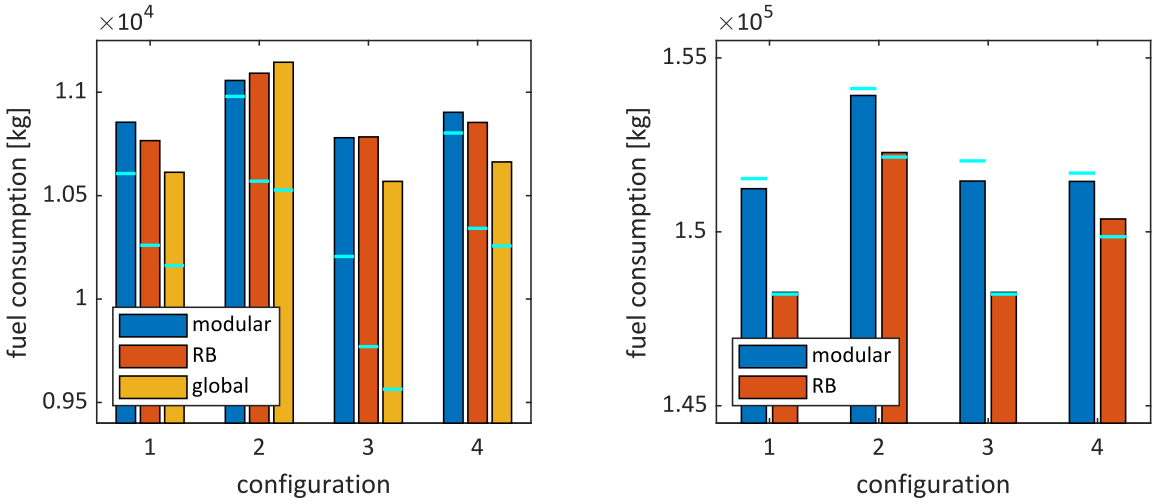

Figure 34 corrected fuel consumption for tested EMSs for all configurations, for operating profile 1 (left) and 2 (right). Uncorrected fuel consumption is shown with the cyan lines.

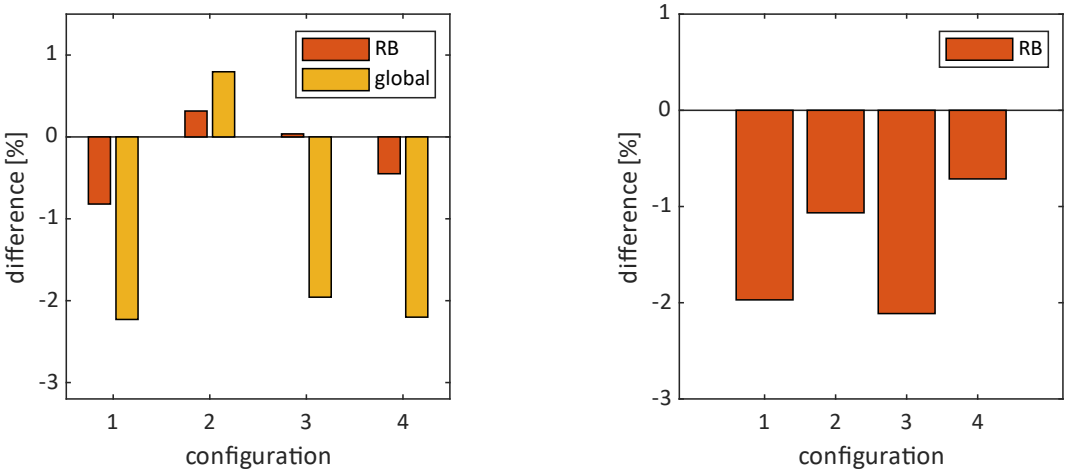

Figure 35 corrected fuel consumption of the developed EMS relative to the benchmark EMSs, for operating profile 1 (left) and 2 (right)

For each configuration, there was an expectation for the corrected fuel consumption to be higher or lower, compared to configuration 1:

- Configuration 2: higher, because of the lower efficiency of the HP genset.
- Configuration 3: lower, because the larger batteries would allow the gensets to run more efficiently, more often.
- Configuration 4: higher, because there are fewer power levels where all active gensets can be run at high efficiency.

From the results shown in Table 9 it is concluded that these expectations were correct, with the exception of configuration 3 during OP 2. This is likely because one of the less efficient gensets needs to be active for longer (compared to configuration 1) to be able to re-charge the batteries.

It is clear that the global optimization performs best in terms of uncorrected fuel consumption. Because it drains the battery, the corrected fuel consumption is significantly higher than the uncorrected. For configuration 2 this even leads to a higher corrected consumption than that of the other methods. For the tested conditions, except for configuration 2, the MPS EMS uses 1.9-2.3% more fuel than the global optimization. This is comparable to the results found in literature where ECMS is compared to a global optimization [39], [40], [44].

When compared to the RB EMS, the developed EMS uses between 0.3% less, and 0.8% more fuel for OP 1. For OP 2 it uses 1.1-2.1% more fuel. This higher fuel consumption is most likely due to the inaccuracy of the quadratic approximation of the gensets at high power (Figure 13), which leads the MPS EMS to run the (LP) gensets at high power, where they are relatively inefficient, to charge the batteries.

5.3.4 Component failure

To show the developed EMS will keep operating when one of the components fails during a voyage, simulations were run where a component is disconnected during the voyage. This was done for configuration 1, operating profile 1. The component which was disconnected, was the component which was active longest originally: LP genset 2.

Multiple simulations were run, where the genset was disconnected at a different timepoint in the voyage: 0%, 25%, 50%, and 75% of the voyage duration. This equates to 0, 9, 18, and 27 hours into the voyage. The results are plotted in Figure 36-39. In these figures a vertical line is shown to indicate the point where the genset fails.

It is important to note that it is possible to drain the batteries past their allowed minimum SoC when the available genset power is lower than the required power. When LP genset 2 is unavailable, the remaining available genset power is 3405 kW. This is less than the required power at three time intervals during operating profile 1. Because these time intervals are quite short, and the batteries were sufficiently charged when they started, the batteries were never drained too far during the tested conditions.

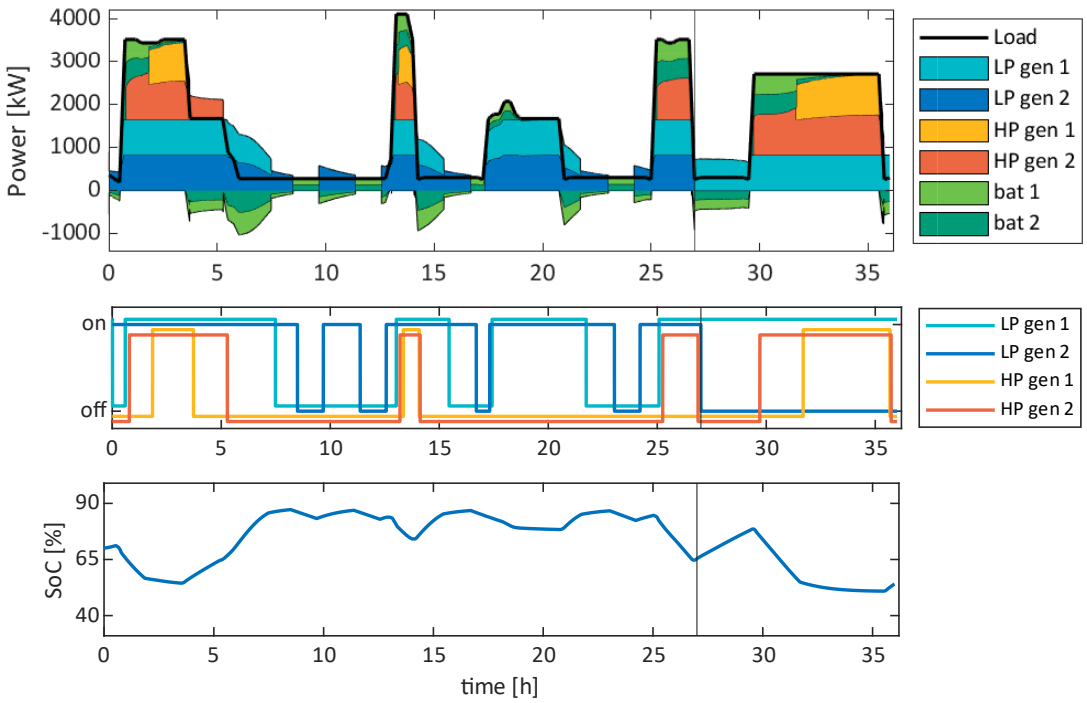

Figure 36 simulation results for hardware configuration 1, and OP 1, when LP genset 2 fails at t = 27 [h]

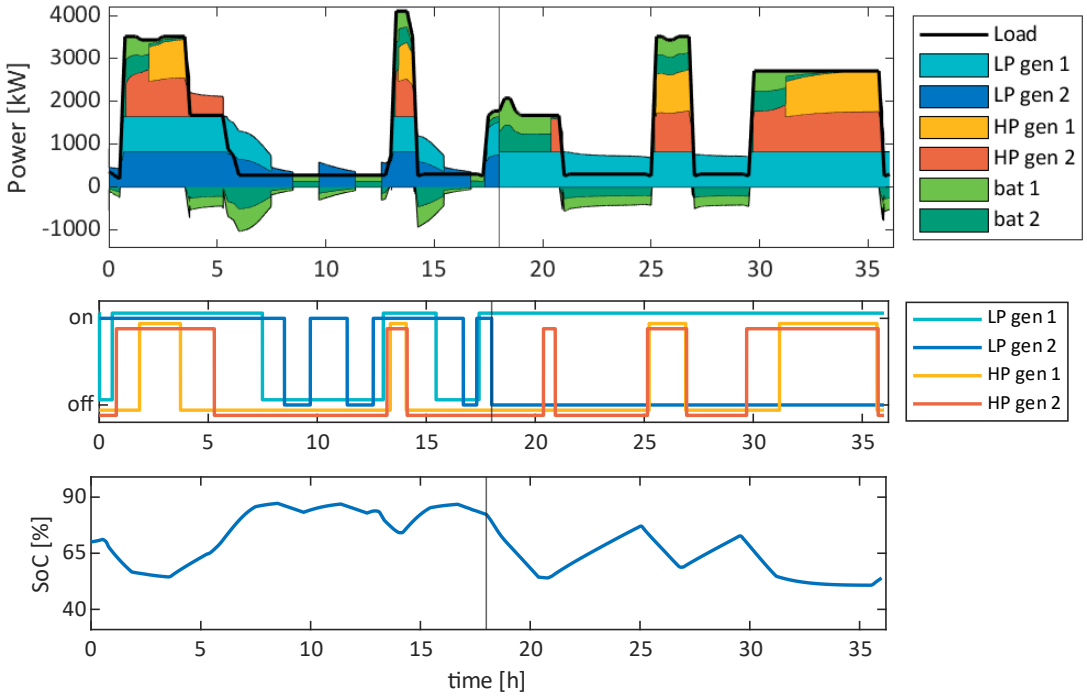

Figure 37 simulation results for hardware configuration 1, and OP 1, when LP genset 2 fails at t = 18 [h]

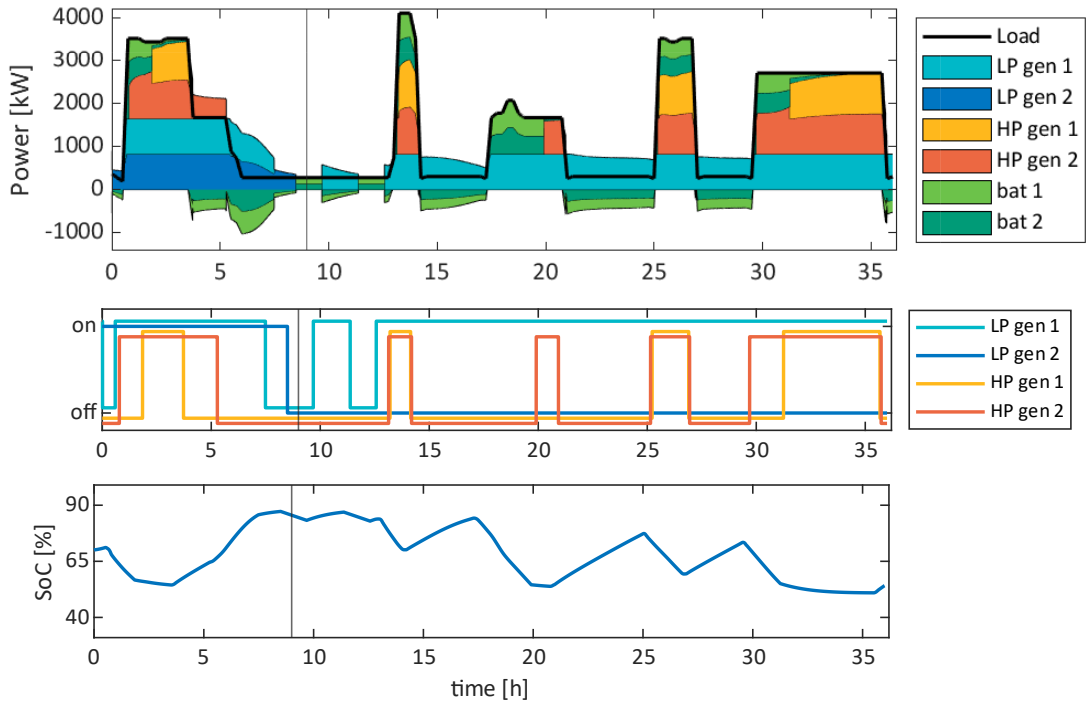

Figure 38 simulation results for hardware configuration 1, and OP 1, when LP genset 2 fails at t = 9 [h]

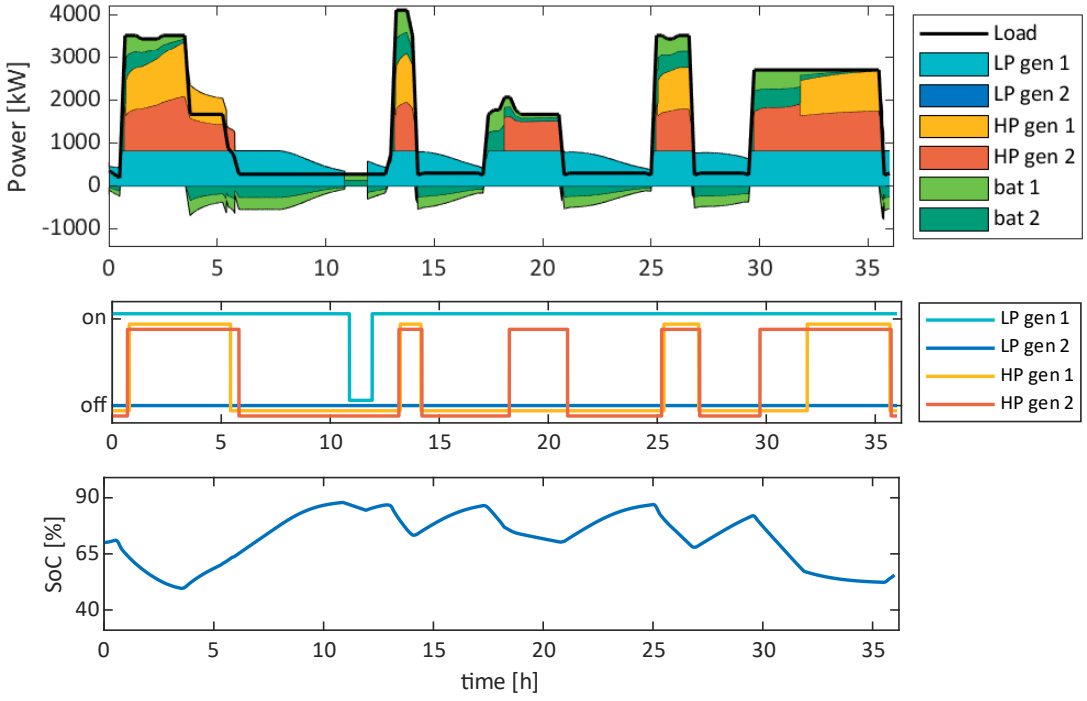

Figure 39 simulation results for hardware configuration 1, and OP 1, when LP genset 2 fails at t = 0 [h]

The fuel consumption for these scenarios is given in Table 10. The fuel consumption when no failure occurs is also included for comparison. Figure 40 gives a visual representation of this data, and also shows the relative increase in fuel consumption, when compared to regular operation.

Where previously both LP gensets were active, now the batteries will be used to compensate for the failed genset, until the SoC drops to a certain level. Then an HP genset will be activated. At the points where previously only one HP genset was active, now two will be active. When the required power drops, the remaining LP genset is kept active to recharge the batteries.

The fuel consumption shows a clear trend: it increases as LP genset 2 fails sooner in the voyage. This indicates that when LP genset 2 is available, the EMS will only activate it when it is the most fuel efficient option. This shows the EMS is capable of minimizing the instantaneous fuel consumption, even when the hardware configuration changes during a voyage. This also applies to changing the installed components of an MPS.

Table 10 fuel consumption [kg] when LP genset 2 fails during the voyage

Failure time [h]	Fuel	Cor fuel
0	10675	10921
9	10606	10874
18	10594	10867
27	10597	10865
-	10607	10855

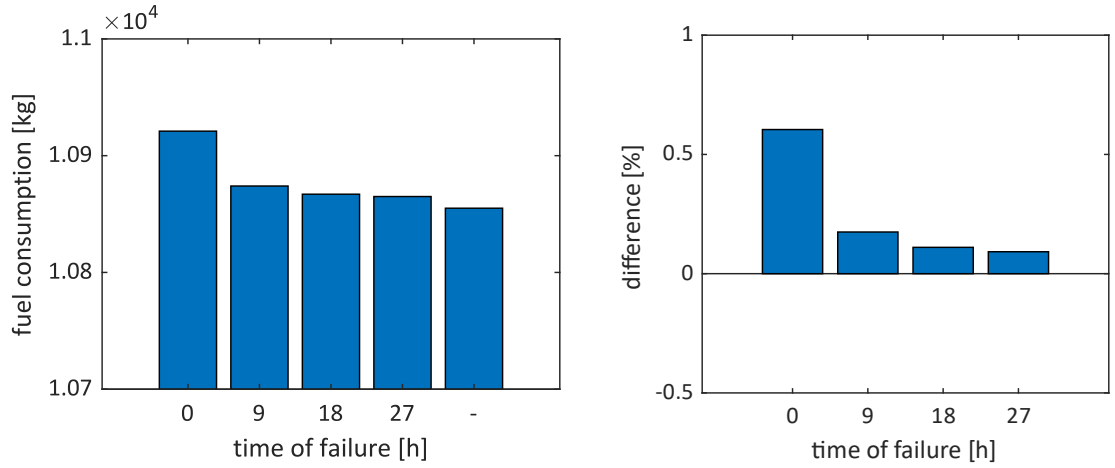

Figure 40 fuel consumption (left) and relative fuel consumption (right), when LP genset 2 fails during OP1

5.4 Discussion

Most importantly, the MPS EMS was able to control the system for all tested situations, while keeping all components within their allowed operating ranges, even when one of the components became unavailable during the voyage. Furthermore, fuel consumption was as expected, compared to a global optimization, as it was similar to the results found in literature where ECMS is compared to a global optimization. However, some behaviors were observed, which could be improved upon.

First of which is the power split when both LP and HP gensets are active. The LP genset(s) will run at maximum power, even though this is often less fuel efficient than transferring some of the power demand to the HP genset(s). This is caused by the inaccuracy (at high power levels) of the

approximated efficiency curve shown in Figure 9. With the approximation, the EMS is told that the LP genset is more efficient at full power, than the HP genset at any power level, which is not actually the case. This issue is especially present during OP 2. It explains the increased fuel consumption compared to the RB EMS. Improving the accuracy of the efficiency curve the EMS uses will decrease overall fuel consumption. In this case, it would also reduce the wear on the LP gensets. However, it is important that the improving this accuracy is not allowed to affect the convexity of the function.

Another factor which causes increased genset power demand, is the base value of the equivalent cost factor (equation (*5*)). Because it is based on the average BSFC, it will increase if the gensets are operated at inefficient operating points. Consequently, the increased equivalent cost factor will allow the gensets to run less efficiently before battery power is preferred, which will increase it even further. This is also the case when the less efficient HP gensets are used, compared to when only LP gensets are used. This is best seen by the difference between configurations 1 and 3, in OP 1 from 18-21 hours. Because configuration 3 makes less use of the HP gensets before this point, the equivalent cost factor is slightly lower. Consequently, the LP gensets are run at a lower, more fuel efficient power output, while also using battery power. To prevent the equivalent cost factor from becoming higher than necessary, the method for determining its value should be adjusted.

6 Conclusion

With an MPS it is possible to choose which components are installed, such that their capabilities best match the requirements of the upcoming voyage. The control system of an MPS needs to be able to adapt when the type and number of installed components changes. For this thesis an MPS EMS was developed: an EMS capable of dealing with a reconfigurable power plant, where components can be added, removed, or replaced. This EMS also needed to be able to minimize fuel consumption, regardless of the operating profile, and which components are installed. Another requirement was that the EMS be real-time capable. The developed MPS EMS is meant for ships with electric propulsion and a hybrid power plant, but can also be used for other applications. It can be used as a benchmark during development of a bespoke EMS, or as a tool to find a good power plant configuration during the development of a vessel. Another use case is in retrofitted vessels, bypassing the need to develop a bespoke EMS and the associated costs.

The first sub research question, *'what control strategy is suited for an MPS EMS?'*, was answered with a literature study. From the literature study it was found that ECMS would be suited for an MPS EMS, when combined with the dual decomposition method. Dual decomposition makes it possible to uncouple the power balance constraints of each component. This means components can be added, removed, or replaced, without affecting the equations of the other components.

Now the second sub research question, '*how can a variable number/type of connected components be represented in the controller?',* can be answered. To determine the optimal power split between the connected components, the EMS needs to know certain properties of these components, such as their efficiency curve and maximum power. The data of these properties is integrated into the individual components. The connected components will then communicate this data, and thus their properties, to the EMS. This way, connecting a different component will automatically give the EMS the information it needs to include this component in the optimization. Because the MPS EMS needs to work for a variety of installed components and operating profiles, certain parameters need to adapt automatically. To ensure the steepest ascend method (used to find the correct power split) converges quickly and stably for all component configurations, the starting point and step size of the iterations are made adaptive. To make sure the batteries do not exceed their SoC limits, the equivalent cost factor was made adaptive as well.

The answer to third sub research question, *'how can the performance of the developed EMS be assessed?',* determined which test scenarios the MPS EMS was subjected to. The results needed to show the capabilities of the developed EMS for its two main objectives: dealing with an MPS, and minimizing fuel consumption. Therefore simulations were performed with four different hardware configurations, and two different operating profiles. All tests were performed without manually changing any control parameters, or other aspects of the EMS. To show the capabilities of the developed EMS in terms of minimizing fuel consumption, an RB EMS and a global optimization were used as benchmarks. Lastly, it was tested how the developed EMS would cope with a genset failure during a voyage. This was tested because an MPS EMS should automatically adjust, and continue operating with the new hardware configuration.

The simulation results show that the MPS EMS was able to control the system for all tested situations, while keeping all components within their allowed operating ranges. The MPS EMS achieved this without the need for any manual adjustments. Fuel consumption relative to a global optimization was similar to results found in literature. Compared to a CD/CS based RB EMS, the fuel consumption was between 0.3% lower, and 2.1% higher. Even though minimizing fuel

consumption could be improved, fuel consumption was not unreasonably high. Hence, the main goal of this thesis was achieved: to develop an EMS capable of controlling a shipboard modular power system, while minimizing fuel consumption.

One way to improve the minimization of fuel consumption, is to improve the accuracy of the approximation of the efficiency curves of the gensets, particularly at high power output. Improving this would reduce the time of running the gensets at, relatively inefficient, high power output. A possible way of doing this would be to implement a piecewise approximation. The second thing that could be improved is the method for determining the base value of the equivalent cost factor, λ_0. Because the used method is based on the average fuel efficiency, it is possible that λ_0 becomes higher than desired if the gensets are, at some point, used at inefficient operating points. Improving this would (further) discourage the EMS from running the gensets at inefficient operating points. A possible solution would be to let λ_0 depend on the efficiency of the desired operating range of the gensets. Neither of the issues mentioned above impact the EMSs ability to stably control an MPS, but they can increase fuel consumption.

6.1 Future works

Future research has various directions it could focus on. One of which is the inclusion of other power sources, such as fuel cells. The ability to handle many different types of components (simultaneously) would further diversify the use cases where the MPS EMS can be applied. Specifically, attention should be paid to how the equivalent cost factor should be implemented when using multiple fuel types.

Another research direction would be to expand the capabilities of the MPS EMS to work for hybrid propulsion systems as well. This would mainly involve expanding the balance equations to include multiple nodes, instead of the single node for electric propulsion, as shown in Figure 12.

The inclusion and effect of component degradation is also a possible topic for future research. Real world scenarios will always suffer from component degradation. Making sure the MPS EMS can deal with this is crucial if it is ever to be applied on existing vessels.

Bibliography

[1] 'Feadship Obsidian yacht 2023', Feadship | Obsidian. Accessed: Aug. 13, 2024. [Online]. Available: https://www.feadship.nl/fleet/obsidian

[2] S. A. Shaheen and T. E. Lipman, 'Reducing Greenhouse Emissions And Fuel Consumption', *IATSS Research*, vol. 31, no. 1, pp. 6–20, 2007, doi: 10.1016/S0386-1112(14)60179-5.

[3] H. Winnes, L. Styhre, and E. Fridell, 'Reducing GHG emissions from ships in port areas', *Research in Transportation Business & Management*, vol. 17, pp. 73–82, Dec. 2015, doi: 10.1016/j.rtbm.2015.10.008.

[4] IMO, *International convention for the prevention of pollution from ships (MARPOL) annex VI. Consolidated edition. IMO*, 2011.

[5] R. D. Geertsma, R. R. Negenborn, K. Visser, and J. J. Hopman, 'Design and control of hybrid power and propulsion systems for smart ships: A review of developments', *Applied Energy*, vol. 194, pp. 30–54, May 2017, doi: 10.1016/j.apenergy.2017.02.060.

[6] G. Castles, G. Reed, A. Bendre, and R. Pitsch, 'Economic benefits of hybrid drive propulsion for naval ships', in *2009 IEEE Electric Ship Technologies Symposium*, Baltimore, MD, USA: IEEE, Apr. 2009, pp. 515–520. doi: 10.1109/ESTS.2009.4906560.

[7] N. Planakis, G. Papalambrou, and N. Kyrtatos, 'Predictive power-split system of hybrid ship propulsion for energy management and emissions reduction', *Control Engineering Practice*, vol. 111, p. 104795, Jun. 2021, doi: 10.1016/j.conengprac.2021.104795.

[8] B. Zahedi, L. E. Norum, and K. B. Ludvigsen, 'Optimized efficiency of all-electric ships by dc hybrid power systems', *Journal of Power Sources*, vol. 255, pp. 341–354, Jun. 2014, doi: 10.1016/j.jpowsour.2014.01.031.

[9] O. B. Inal, J.-F. Charpentier, and C. Deniz, 'Hybrid power and propulsion systems for ships: Current status and future challenges', *Renewable and Sustainable Energy Reviews*, vol. 156, p. 111965, Mar. 2022, doi: 10.1016/j.rser.2021.111965.

[10] Canadian Coastguard and P. J. Hanbidge, 'A Mission-Driven Approach To Vessel Design', in *Small Craft Safety*, RINA, May 2001, pp. 19–28. doi: 10.3940/rina.sc.2001.03.

[11] van Benten, M, Kougiatsos, N, and Reppa, V, 'Mission-oriented Modular Control of Retrofittable Marine Power Plants', preprint, Nov. 2022. doi: 10.24868/10721.

[12] F. J. Vivas, A. De Las Heras, F. Segura, and J. M. Andújar, 'A review of energy management strategies for renewable hybrid energy systems with hydrogen backup', *Renewable and Sustainable Energy Reviews*, vol. 82, pp. 126–155, Feb. 2018, doi: 10.1016/j.rser.2017.09.014.

[13] P. Xie *et al.*, 'Optimization-Based Power and Energy Management System in Shipboard Microgrid: A Review', *IEEE Systems Journal*, vol. 16, no. 1, pp. 578–590, Mar. 2022, doi: 10.1109/JSYST.2020.3047673.

[14] 'MENENS', Methanol powered shipping. Accessed: Aug. 16, 2024. [Online]. Available: menens.nl

[15] W. van Schie, 'Literature study: EMS control strategies suited for modular power systems in ships', unpublished, Mar. 2024.

[16] J. F. Hansen and F. Wendt, 'History and State of the Art in Commercial Electric Ship Propulsion, Integrated Power Systems, and Future Trends', *Proc. IEEE*, vol. 103, no. 12, pp. 2229–2242, Dec. 2015, doi: 10.1109/JPROC.2015.2458990.

[17] R. D. Geertsma, 'Autonomous Control for Adaptive Ships: with Hybrid Propulsion and Power Generation', Delft University of Technology, 2019. doi: 10.4233/UUID:AD81B0EE-76BE-4054-A7E8-BD2EEECDB156.

[18] S. Kanerva and J.-F. Hansen, 'State of the art in electric propulsion - viewpoint on redundancy', in *2009 IEEE Electric Ship Technologies Symposium*, Baltimore, MD, USA: IEEE, Apr. 2009, pp. 499–504. doi: 10.1109/ESTS.2009.4906558.

[19] T. P. Fletcher, 'Optimal energy management strategy for a fuel cell hybrid electric vehicle', Loughborough University, 2017. [Online]. Available: https://hdl.handle.net/2134/25567

[20] A. K. Soltani, M. Kandidayeni, L. Boulon, and D. L. St-Pierre, 'Modular Energy Systems in Vehicular Applications', *Energy Procedia*, vol. 162, pp. 14–23, Apr. 2019, doi: 10.1016/j.egypro.2019.04.003.
[21] A. S. Mohammed, S. M. Atnaw, A. O. Salau, and J. N. Eneh, 'Review of optimal sizing and power management strategies for fuel cell/battery/super capacitor hybrid electric vehicles', *Energy Reports*, vol. 9, pp. 2213–2228, Dec. 2023, doi: 10.1016/j.egyr.2023.01.042.
[22] Y. Cao, M. Yao, and X. Sun, 'An Overview of Modelling and Energy Management Strategies for Hybrid Electric Vehicles', *Applied Sciences*, vol. 13, no. 10, p. 5947, May 2023, doi: 10.3390/app13105947.
[23] S. Onori, L. Serrao, and G. Rizzoni, *Hybrid Electric Vehicles*. in SpringerBriefs in Electrical and Computer Engineering. London: Springer London, 2016. doi: 10.1007/978-1-4471-6781-5.
[24] Chan-Chiao Lin, Huei Peng, J. W. Grizzle, and Jun-Mo Kang, 'Power management strategy for a parallel hybrid electric truck', *IEEE Trans. Contr. Syst. Technol.*, vol. 11, no. 6, pp. 839–849, Nov. 2003, doi: 10.1109/TCST.2003.815606.
[25] T. C. J. Romijn, T. H. Pham, and S. Wilkins, 'Modular ECMS Framework for Hybrid Vehicles', *IFAC-PapersOnLine*, vol. 52, no. 5, pp. 128–133, 2019, doi: 10.1016/j.ifacol.2019.09.021.
[26] H. Yu, D. Tarsitano, X. Hu, and F. Cheli, 'Real time energy management strategy for a fast charging electric urban bus powered by hybrid energy storage system', *Energy*, vol. 112, pp. 322–331, Oct. 2016, doi: 10.1016/j.energy.2016.06.084.
[27] A. Schell, H. Peng, D. Tran, E. Stamos, C.-C. Lin, and M. J. Kim, 'Modelling and control strategy development for fuel cell electric vehicles', *Annual Reviews in Control*, vol. 29, no. 1, pp. 159–168, Jan. 2005, doi: 10.1016/j.arcontrol.2005.02.001.
[28] W. Wang, Z. Cai, and S. Liu, 'Design of Real-Time Control Based on DP and ECMS for PHEVs', *Mathematical Problems in Engineering*, vol. 2021, pp. 1–12, Feb. 2021, doi: 10.1155/2021/6667614.
[29] S. Onori and L. Tribioli, 'Adaptive Pontryagin's Minimum Principle supervisory controller design for the plug-in hybrid GM Chevrolet Volt', *Applied Energy*, vol. 147, pp. 224–234, Jun. 2015, doi: 10.1016/j.apenergy.2015.01.021.
[30] C. Hou, M. Ouyang, L. Xu, and H. Wang, 'Approximate Pontryagin's minimum principle applied to the energy management of plug-in hybrid electric vehicles', *Applied Energy*, vol. 115, pp. 174–189, Feb. 2014, doi: 10.1016/j.apenergy.2013.11.002.
[31] N. Sulaiman, M. A. Hannan, A. Mohamed, P. J. Ker, E. H. Majlan, and W. R. Wan Daud, 'Optimization of energy management system for fuel-cell hybrid electric vehicles: Issues and recommendations', *Applied Energy*, vol. 228, pp. 2061–2079, Oct. 2018, doi: 10.1016/j.apenergy.2018.07.087.
[32] X. Wang, U. Shipurkar, A. Haseltalab, H. Polinder, F. Claeys, and R. R. Negenborn, 'Sizing and Control of a Hybrid Ship Propulsion System Using Multi-Objective Double-Layer Optimization', *IEEE Access*, vol. 9, pp. 72587–72601, 2021, doi: 10.1109/ACCESS.2021.3080195.
[33] F. Teng, Q. Zhang, G. Xiao, Z. Ban, Y. Liang, and Y. Guan, 'Energy Management for a Port Integrated Energy System Based on Distributed Dual Decomposition Mixed Integer Linear Programming', *JMSE*, vol. 11, no. 6, p. 1137, May 2023, doi: 10.3390/jmse11061137.
[34] Z. Li, Y. Xu, S. Fang, X. Zheng, and X. Feng, 'Robust Coordination of a Hybrid AC/DC Multi-Energy Ship Microgrid With Flexible Voyage and Thermal Loads', *IEEE Trans. Smart Grid*, vol. 11, no. 4, pp. 2782–2793, Jul. 2020, doi: 10.1109/TSG.2020.2964831.
[35] P. Rozier and J. M. Tarascon, 'Review—Li-Rich Layered Oxide Cathodes for Next-Generation Li-Ion Batteries: Chances and Challenges', *J. Electrochem. Soc.*, vol. 162, no. 14, pp. A2490–A2499, 2015, doi: 10.1149/2.0111514jes.
[36] T. C. J. Romijn, M. C. F. Donkers, J. T. B. A. Kessels, and S. Weiland, 'A Distributed Optimization Approach for Complete Vehicle Energy Management', *IEEE Trans. Contr. Syst. Technol.*, vol. 27, no. 3, pp. 964–980, May 2019, doi: 10.1109/TCST.2018.2789464.

[37] C. Musardo, G. Rizzoni, Y. Guezennec, and B. Staccia, 'A-ECMS: An Adaptive Algorithm for Hybrid Electric Vehicle Energy Management', *European Journal of Control*, vol. 11, no. 4–5, pp. 509–524, Jan. 2005, doi: 10.3166/ejc.11.509-524.
[38] D. Yao *et al.*, 'Adaptive Equivalent Fuel Consumption Minimization Based Energy Management Strategy for Extended-Range Electric Vehicle', *Sustainability*, vol. 15, no. 5, p. 4607, Mar. 2023, doi: 10.3390/su15054607.
[39] M. Kalikatzarakis, R. D. Geertsma, E. J. Boonen, K. Visser, and R. R. Negenborn, 'Ship energy management for hybrid propulsion and power supply with shore charging', *Control Engineering Practice*, vol. 76, pp. 133–154, Jul. 2018, doi: 10.1016/j.conengprac.2018.04.009.
[40] J. Zhu, L. Chen, X. Wang, and L. Yu, 'Bi-level optimal sizing and energy management of hybrid electric propulsion systems', *Applied Energy*, vol. 260, p. 114134, Feb. 2020, doi: 10.1016/j.apenergy.2019.114134.
[41] G. B. Dantzig and P. Wolfe, 'The Decomposition Algorithm for Linear Programs', *Econometrica*, vol. 29, no. 4, p. 767, Oct. 1961, doi: 10.2307/1911818.
[42] A. Rantzer, 'Dynamic dual decomposition for distributed control', in *2009 American Control Conference*, St. Louis, MO, USA: IEEE, 2009, pp. 884–888. doi: 10.1109/ACC.2009.5160224.
[43] A. Kozma, J. V. Frasch, and M. Diehl, 'A distributed method for convex quadratic programming problems arising in optimal control of distributed systems', in *52nd IEEE Conference on Decision and Control*, Firenze: IEEE, Dec. 2013, pp. 1526–1531. doi: 10.1109/CDC.2013.6760099.
[44] H. Chen, J. T. B. A. Kessels, and S. Weiland, 'Adaptive ECMS: a Causal Set-theoretic Method for Equivalence Factor Estimation', *IFAC-PapersOnLine*, vol. 48, no. 15, pp. 78–85, 2015, doi: 10.1016/j.ifacol.2015.10.012.

Appendices

A Results RB EMS

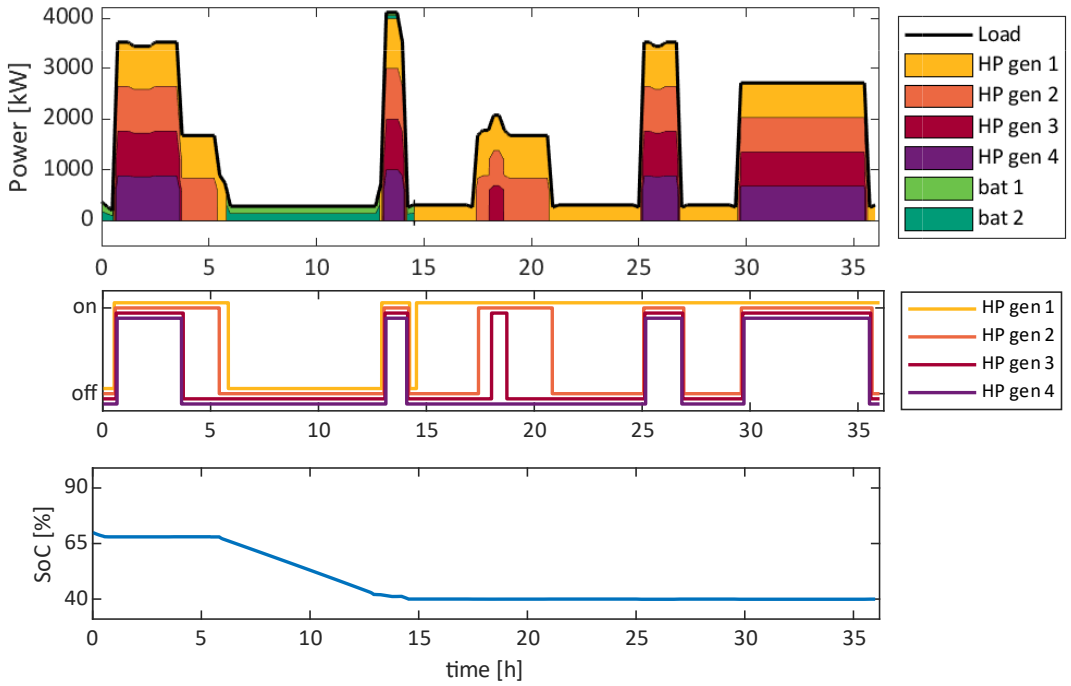

Figure A-1 simulation results for hardware configuration 2, and OP 1, with the RB EMS

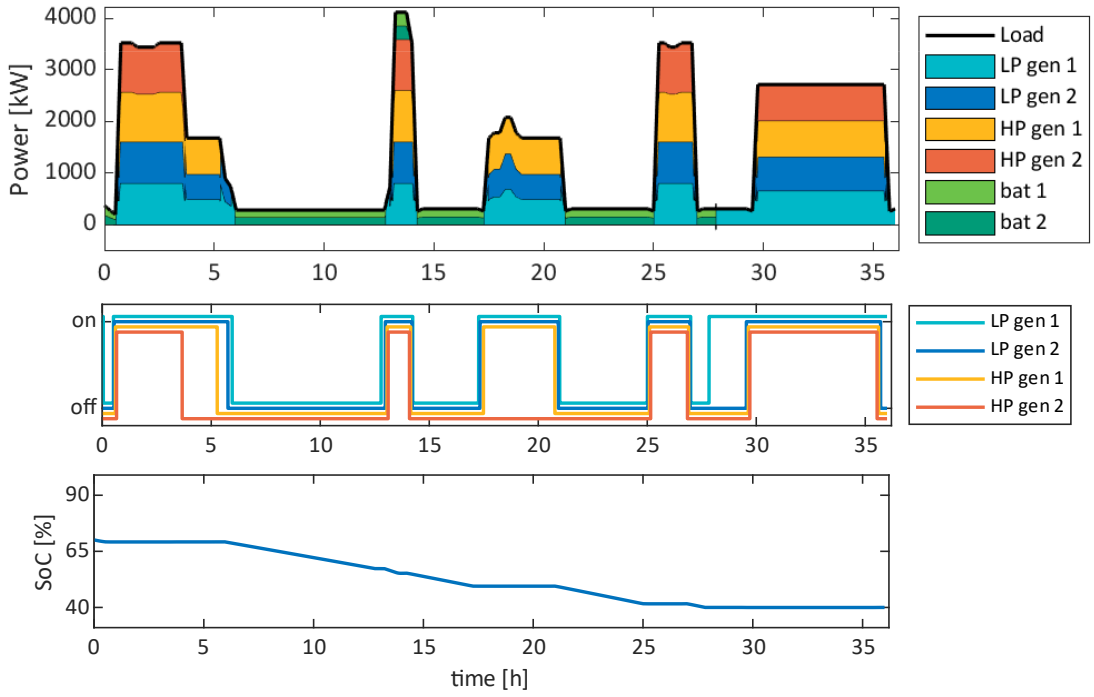

Figure A-2 simulation results for hardware configuration 3, and OP 1 , with the RB EMS

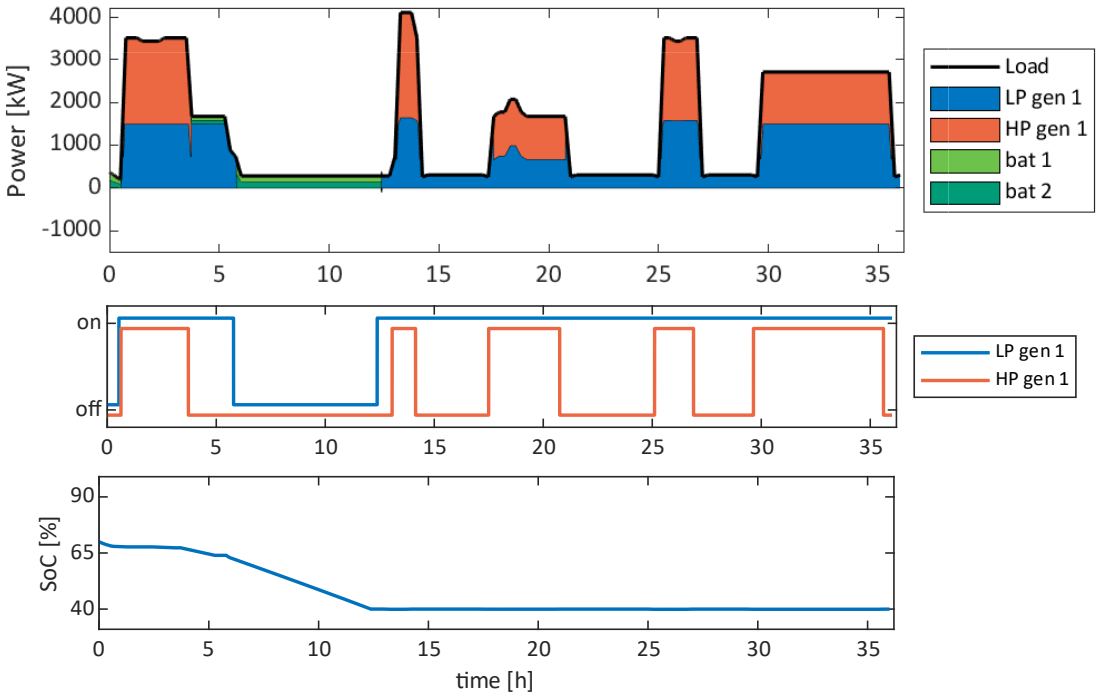

Figure A-3 simulation results for hardware configuration 4, and OP 1 , with the RB EMS

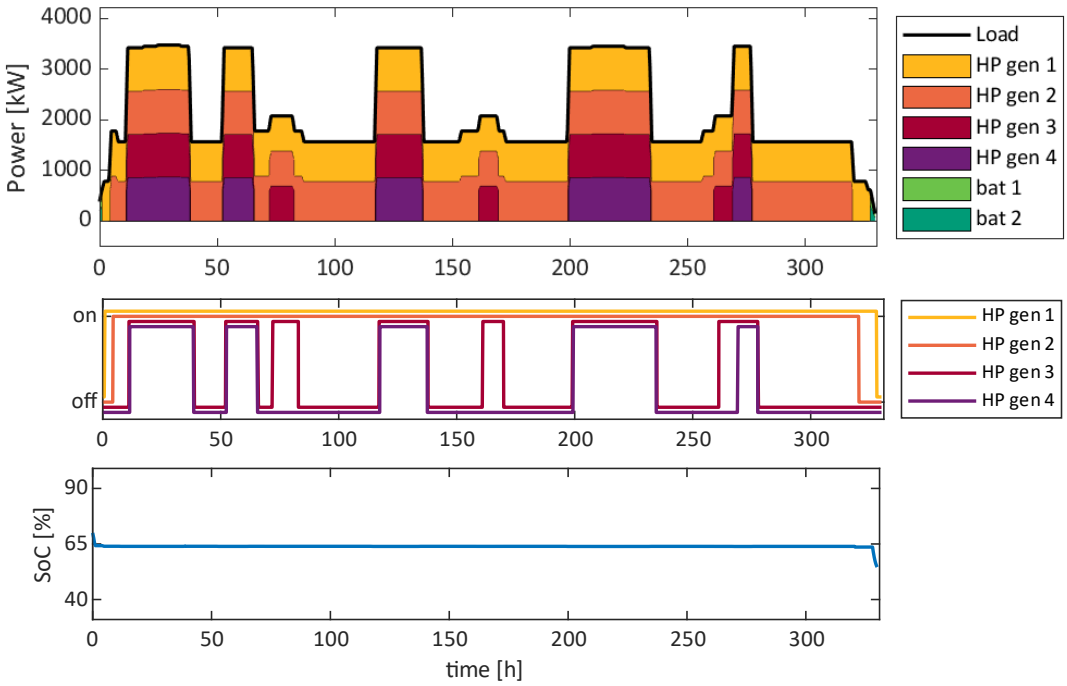

Figure A-4 simulation results for hardware configuration 2, and OP 2, with the RB EMS

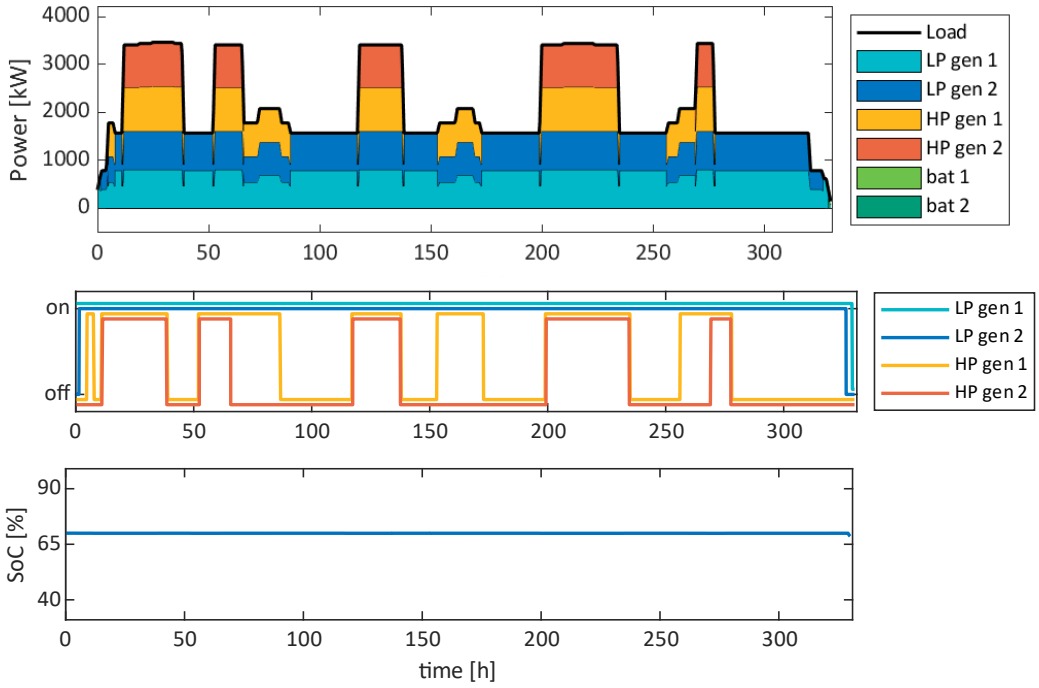

Figure A-5 simulation results for hardware configuration 3, and OP 2, with the RB EMS

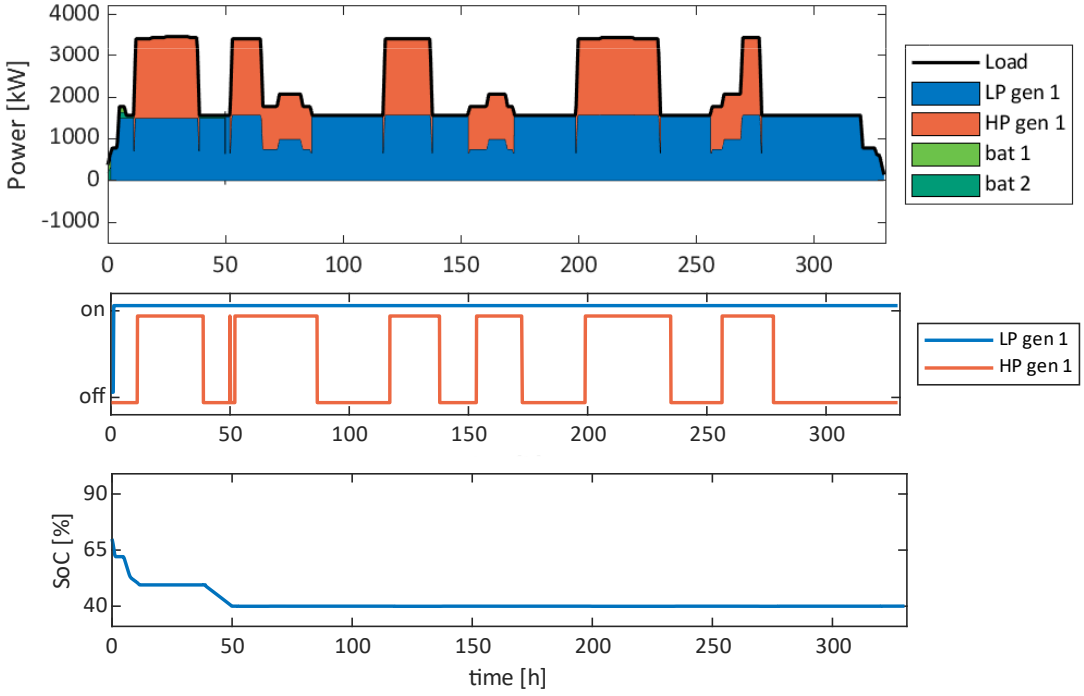

Figure A-6 simulation results for hardware configuration 4, and OP 2 , with the RB EMS

B Results global optimization

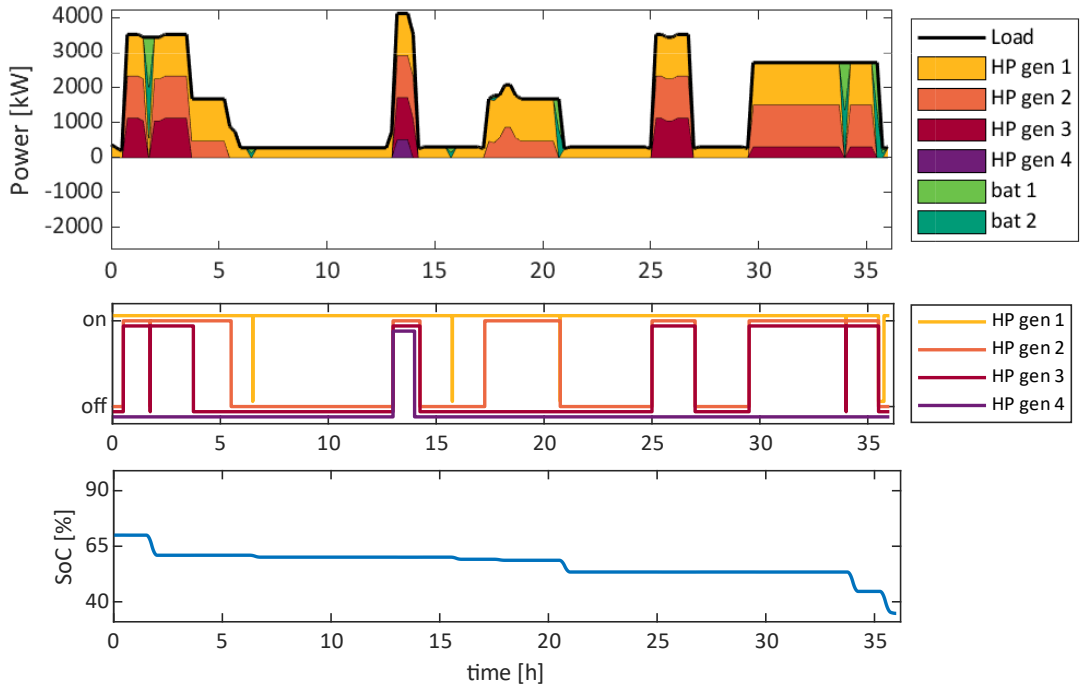

Figure B-1 simulation results for hardware configuration 2, and OP 1, with the MILP global optimization

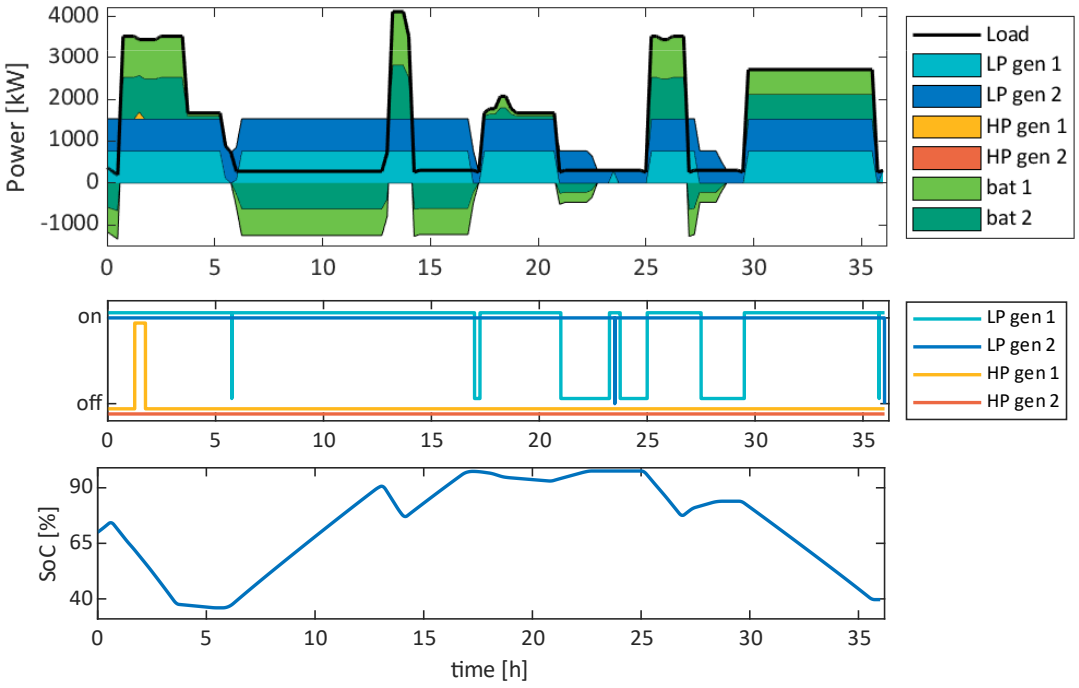

Figure B-2 simulation results for hardware configuration 3, and OP 1, with the MILP global optimization

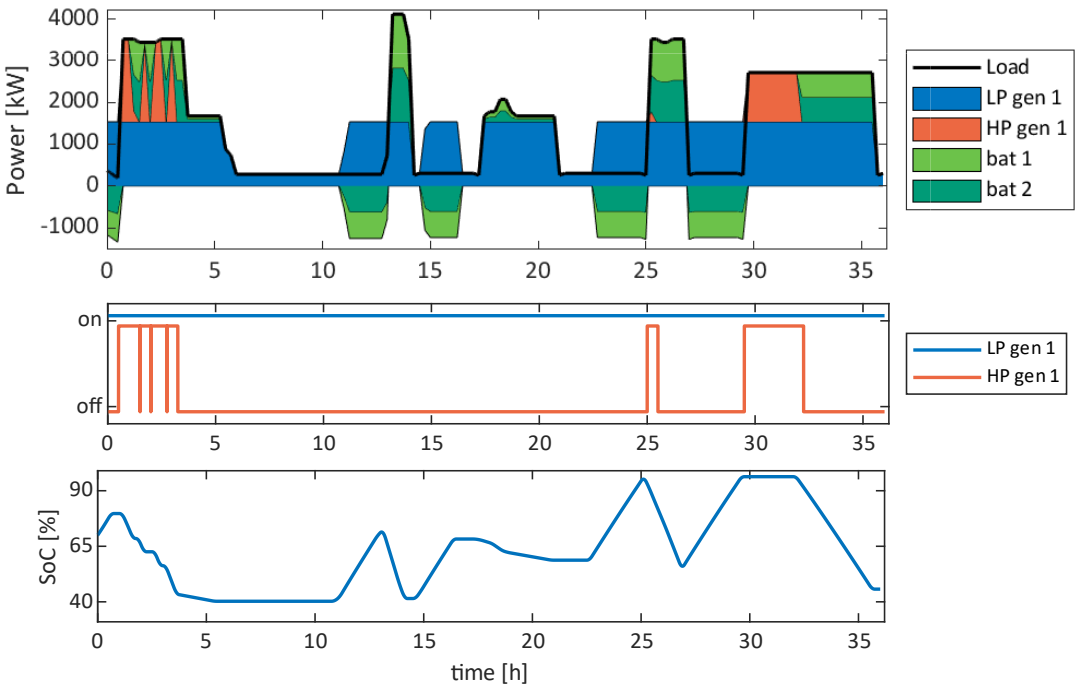

Figure B-3 simulation results for hardware configuration 4, and OP 1, with the MILP global optimization